2007

Modeling the Cumulative Effects of Forest Fire on Watershed Hydrology: A Post-fire Application of the Distributed Hydrology-Soil-Vegetation Model (DHSVM)

Crystal S. Stonesifer
The University of Montana

MODELING THE CUMULATIVE EFFECTS OF FOREST FIRE ON WATERSHED HYDROLOGY: A POST-FIRE APPLICATION OF THE DISTRIBUTED HYDROLOGY-SOIL-VEGETATION MODEL (DHSVM)

By

Crystal S. Stonesifer

B.S., Resource Conservation, University of Montana, Missoula, MT, 2002

Thesis

presented in partial fulfillment of the requirements
for the degree of

Master of Science
in Resource Conservation

The University of Montana
Missoula, MT

Spring 2007

Approved by:

Dr. David A. Strobel, Dean
Graduate School

Dr. Donald Potts, Chair
Department of Society and Conservation

Dr. LLoyd Queen
Department of Forest Management

Dr. Joel Henry
Department of Computer Science

Stonesifer, Crystal S., M.S., Spring 2007 Resource Conservation

Modeling the Cumulative Effects of Forest Fire on Watershed Hydrology: A Post-fire Application of the Distributed Hydrology-Soil-Vegetation Model (DHSVM)

Chairperson: Dr. Donald Potts

Abstract.

The Distributed Hydrology-Soil-Vegetation Model (DHSVM) was applied to the Eightmile Creek watershed in western Montana. The purpose of this research was primarily to assess the applicability of the model as a cumulative effects assessment tool in the post-fire landscape of a forested watershed in this region. The model was first calibrated to the pre-fire watershed conditions using six years of historic streamflow data. DHSVM was able to accurately simulate the general shape of the measured hydrograph for each of the six simulated water years, and the normalized median absolute error statistics were below the target threshold of 50% for each year simulated. This relative success of the calibration efforts is particularly surprising when one considers the significant limitations presented by the lack of any sub-daily or high-elevation meteorological data for use in driving the calibration simulations. Because the accuracy of DHSVM simulations were greatly improved through rigorous calibration, this research demonstrates the need for model calibration to a watershed of interest, prior to hydrologic simulations of different landscape scenarios. Next, two different calibrated versions of DHSVM, including DHSVM version 2.0.1 and the DHSVM fire model, were each used to simulate runoff in the Eightmile Creek watershed following a near catchment-wide stand-replacing forest fire. Due to weather anomalies and limited, discontinuous streamflow data, no decisive conclusions could be made regarding the performance of either version of the model in the validation efforts. Results do suggest, though, that the DHSVM fire model has the potential to outperform the standard model version in fire-affected landscapes. Further research utilizing the DHSVM fire model with more substantial post-fire streamflow records for model validation is warranted.

Acknowledgements.

I am grateful to the National Center for Landscape Fire Analysis for generously funding this research and for providing unlimited opportunities for education, training, work-related experience, and social outings. I would like extend special thanks to the following individuals: Eric Tangedahl for helping me overcome the DHSVM learning curve; Casey Teske for her invaluable AML and editing expertise; Jim Riddering and Carl Seielstad for their tolerant general advising support; Casey Teske, Jim Riddering, Josh Rodriguez, and Eric Rowell for their patient and thoughtful input regarding the defense portion of this project; and Saxon Holbrook for his technological assistance. In addition, I am particularly grateful to Andrew Neuschwander and his interest in debugging code in his spare time. Thanks also to each of my committee members, Don Potts, LLoyd Queen, and Joel Henry, for their individual contributions to this project.

TABLE OF CONTENTS

LIST OF FIGURES

LIST OF TABLES

Table Number **Page**

1. INTRODUCTION

In the forested watersheds of the Rocky Mountain West, an inextricable relationship exists between the balance of water and the behavior of fire. The availability of water in the vegetation, soil and air directly affects fire behavior. Conversely, fire disturbances resulting in landscape changes at the watershed scale will ultimately have a direct effect on the movement and availability of water in that watershed. The spatial variability of moisture conditions will shape burn severity patterns, just as the spatial characteristics of the burn severity mosaic will affect watershed hydrology following a fire.

1.1 *CUMULATIVE EFFECTS.* The hydrologic impacts of environmental changes in forested drainages are often evident in the water processes observed at the watershed scale. This fact is somewhat independent from the size of the land area being drained by a particular stream or river system. Because of this, the terms watershed, catchment, and drainage basin can be used interchangeably when discussing cumulative watershed effects, without suggesting a particular scale beyond that of a complete drainage area.

Cumulative watershed effects (CWEs) are the product of the collective impacts of multiple landscape changes within a drainage basin over space or time (MacDonald, 2000). CWEs are influenced by processes involving the generation or transport of water. The primary areas of concern with respect to CWEs are watershed scale changes in runoff, water quality, channel morphology, and aquatic ecosystems (Reid, 1993). The cumulative effects of fire on the timing and intensity of runoff from forested catchments are highly variable and difficult to quantify. The forest plays an important role in the physical processes governing water movement in a catchment, absorbing and storing precipitation, shading the snowpack from the radiative effects of the sun, and stabilizing

channels and slopes. The physical characteristics of vegetative cover greatly influence hydrologic processes. Removal or alteration of the canopy of trees in a forested watershed may lead to increased snow accumulation and melt, decreased evapotranspiration, and a net increase in the stormflow response (Harr *et al.*, 1975; Troendle and King, 1985). Changes to the forest vegetation structure resulting from harvest and associated road building have been shown to affect hydrograph characteristics, leading to earlier, higher intensity peak flows (Harr, 1981; Christner and Harr, 1982; Harr, 1986; Berris and Harr, 1987; Jones and Grant, 1996). Forest fires may effectively alter the vegetation structure at a watershed scale, potentially leading to similar changes in runoff dynamics.

1.2 ***MECHANISM OF LANDSCAPE CHANGE.*** While removal of forest vegetation by any means will tend to alter runoff characteristics in a snow-dominated system, the mechanism of removal affects the types of hydrologic changes that are produced. Road building and harvest may be grouped in the same category, as both practices reduce the canopy cover, thereby affecting snow accumulation and ablation patterns. Roads and skid trails also both behave, in a hydrologic sense, effectively as channels. The network of roads and harvest trails replace preferential subsurface flow paths, routing water quickly across the landscape surface and into the stream network. As a result, the impacts of weather events on the hydrologic system are often more quickly apparent. Streamflow levels rise and subside more rapidly, and peak streamflows tend to increase in overall magnitude (Bowling and Lettenmaier, 1997). Other impacts to the hydrologic system resulting from road building and harvest practices include

increased levels of soil compaction and understory disturbance resulting in potential increases in overland flow and associated soil erosion.

In contrast, landscape changes resulting from forest fire may be dramatically different from those presented by forest management and land use. Fires can create physical, chemical and biological changes in soils that affect hydrologic response in a watershed. Under certain conditions, particularly involving high severity fires on coarse-textured soils with resinous litter, a hydrophobic soil layer can be formed (Agee, 1993). These water repellent soils affect the movement of water through the landscape at the watershed scale, and may contribute to an increase in overland flow and rill erosion. However, limited understanding of the processes governing hydrophobicity formation, persistence and spatial variability leads to difficulty quantifying the hydrologic effects of these soils (DeBano, 2000).

Vegetation changes resulting from fire also differ from those due to forest harvest. Depending on the fire severity, partial to full combustion of the understory and overstory components may occur. Resulting scenarios that are unlikely to be replicated in a harvest situation include full consumption of the understory without canopy disruption and full consumption of the overstory resulting in widespread standing dead timber. Because landscape changes resulting from forest fire are potentially so different from those presented by harvest practices, the tools used to predict the effects of deforestation on hydrologic response for harvest scenarios might not be applicable for management decisions regarding catchments affected by forest fire.

1.3 ***MODELING HIGHLY VARIABLE LANDSCAPES.*** The physical processes governing the hydrologic cycle are generally well understood; however, the ability of

scientists to model these processes is more limited. Complex systems complicated by high degrees of spatial variability in the distribution of soil types, land cover, and meteorological factors are the norm in the mountainous areas of western Montana. Computer models do exist that aim to simulate hydrologic processes following landscape changes. Yet few of these models are capable of accurately representing the spatial variability of landscape features in highly variable terrain, and subsequently, these same models may fail to adequately address the effects of this variability on water movement. Moreover, many of the hydrologic models in use by scientists and land managers were designed to predict the effects of different forest management practices on the hydrology of a catchment. As previously mentioned, these tools may not necessarily be transferable to fire-affected watersheds.

1.4 ***SNOWMELT MODELING.*** The precipitation patterns in a watershed will influence the characteristics of the soils and vegetation found there. The soil and vegetation characteristics, in turn, ultimately control runoff and infiltration processes at the watershed scale (Wohl, 2000). Snow accumulation and ablation patterns play a major role in the hydrologic cycle of coniferous forests in western North America (Waring and Schlesinger, 1985). Accumulation and melt patterns tend to be dependent on physical landscape and forest features, and as a result, are highly spatially variable. Variations in snow cover resulting from canopy interception processes and wind drift around trees may significantly influence surface albedo, melt and runoff (Marsh, 1999). Thus, a distributed snowmelt model must quantitatively address the complex interactions between snow, the forest canopy, and the mountainous landscape at a high enough spatial resolution to adequately capture the spatial variability of the snowpack and accurately simulate

snowmelt. Historically, the existence of such models has been limited by the lack of data necessary to drive these simulations at high spatial resolutions.

In addition, snowmelt models must also address the temporal variability of a dynamic snowpack. For example, snowmelt controlled watersheds tend to exhibit strongly diurnal discharge patterns (Wohl, 2000); therefore, the ability of a simulation tool to calculate water and energy balances at a sub-daily time step is key to accurate modeling of the physical watershed processes in a snow-dominated system. A spatially distributed hydrologic model must also be able to represent the temporal heterogeneity of snow cover in order to accurately model snowmelt in a snow-dominated system.

1.5 ***GENERAL MODEL DESCRIPTIONS.*** Hydrologists have been developing computer applications that model hydrologic response since the mid-1960s (Ward and Elliot, 1995). With the arrival of the personal computer in the 1980s, and with further improvements in processing speeds and storage space, a wide variety of increasingly complex hydrologic models have appeared. In *Mathematical Models of Small Watershed Hydrology and Applications* (Singh and Frevert, 2002) twenty-three different computer based hydrologic models are described. While this is not an exhaustive list, many of the models illustrated represent the most widely used and accepted, as well as the most innovative hydrologic models of the day. At this time, there exists a daunting array of choices of hydrologic simulation tools available to researchers; however, each tool is not appropriate for all objectives, in all scenarios, or every landscape. It is reliant on the discretion of the land manager or researcher to choose the model that is most capable of simulating the landscape processes for the area and scale of interest.

A hydrologic model can essentially be empirical, stochastic or deterministic in nature (Ward and Elliot, 1995). Empirical models rely on observed or experimentally derived data. Also called regression, or "black-box" models, these utilize basic relationships between the inputs and the outputs to model a specific physical process (Grayson and Blöschl, 2000). In comparison, stochastic hydrologic models are essentially statistical models. These employ statistical theory to identify probabilities of specific hydrologic events, such as floods or hillslope failures. Some, or all, of the inputs into a stochastic model are represented by statistical distributions instead of single values (Grayson and Blöschl, 2000). Finally, deterministic models, also described as physically-based models, tend to be the most complex of the three. Here the most important physical and chemical processes taking place on the landscape are represented using mathematical equations. Many of the physical landscape processes are empirically described within the context of the larger deterministic model; therefore, these models are not truly physically-based, but are instead, theoretical in nature (Ward and Elliot, 1995).

Until very recently, few spatially distributed deterministic hydrologic models were in existence (Yeh *et al.*, 2006). These types of models were developed in an attempt to explicitly address the complicated interactions of the atmosphere, topography, soil, water, and vegetation at the watershed scale. Non-distributed, or lumped models, do not explicitly represent the landscape, but instead, utilize average values of watershed characteristics affecting runoff volumes. While this averaging may be a source of significant error in some cases, the advantages of lumped models include low data and computation time demands, relatively simple algorithms, and the resulting high ease of use. In contrast, distributed models tend to be highly input-intensive, and many lack the

user-friendly computer interfaces common among lumped hydrologic models. In addition, if high resolution data is not used in distributed model simulations, the benefits of the spatial and temporal complexity provided by these types of models may be lost. Nevertheless, the lack of complexity in lumped models may come at the cost of accuracy in hydrologic simulations in many cases, particularly in areas with high degrees of spatial and temporal landscape heterogeneity. Because of their ability to address landscape variability, distributed deterministic models may prove particularly effective in modeling the physical processes governing the hydrology of fire-affected, forested landscapes in the western United States, so long as the high-resolution data to drive such simulations is available.

1.6 *THE DISTRIBUTED HYDROLOGY-SOIL-VEGETATION MODEL.* The Distributed Hydrology-Soil-Vegetation Model (DHSVM; Wigmosta *et al.*, 1994; 2002) is a spatially explicit hydrologic model that accounts for the physical processes affecting the movement of water on and through the landscape with a distributed, deterministic approach. In general, the model dynamically represents the spatial distribution of evapotranspiration, snow cover, soil moisture, and runoff across a watershed (Wigmosta *et al.*, 2002). It is theoretically able to simulate runoff, route the movement of sediment and water through the landscape, and pinpoint specific locations prone to mass wasting failure. The sediment routing and mass wasting components have just recently become publicly available with the release of DHSVM version 3.0.

DHSVM solves full water and energy balance equations at the resolution of a digital elevation model (DEM). The DEM provides the foundation for the model structure, and typical spatial resolutions for model applications range from 10- to 100-m (VanShaar *et*

al., 2002). Characterization of soil and vegetation at the DEM resolution drives the topographic controls on absorbed solar radiation, precipitation, air temperature, and downslope water movement in the model (Wigmosta *et al.*, 1994). DHSVM utilizes both a two-layer vegetation representation and a multi-layer soil profile representation. For each pixel within the watershed boundary, a single vegetation type and soil class is assigned. However, the modeler has ultimate control of the parameterization of each soil and vegetation type defined. Any combination or number of individual soil and vegetation classes may be incorporated, thereby enhancing the ability of the modeler to capture landscape variability. The model operates at the time step of the meteorological inputs. It functions at the sub-daily level up to a 1-hr temporal resolution. DHSVM incorporates a sophisticated two-layer snow accumulation and ablation model. Surface and subsurface flow routing algorithms channel water to the watershed outlet and allow grid cells to exchange water with adjacent neighbors (Wigmosta *et al.*, 2002). While DHSVM is not directly linked to any particular Geographical Information System (GIS), the inputs and outputs are best managed within a GIS.

Generally, inputs into DHSVM can be categorized into three separate groups: 1) time series data, 2) spatial data including raster and vector inputs, and 3) associated text files that serve as look-up tables during the modeling process. The time series inputs consist of meteorological data at a specified time step for the period that the model is to be run. Spatial inputs involving raster data include a digital elevation model, a watershed mask, and grids of the vegetation type, soil type, and soil depth, each with the same extent and grid cell resolution. The vector data include arc coverages of the stream and road

networks. The various text file look-up tables provide information about the types of meteorological, soil, and vegetation data used.

DHSVM utilizes a cell-by-cell approach to move water through the hydrologic system. However, there are some inconsistencies in the literature with respect to the actual number of neighbor cells per pixel. Peer reviewed articles, published as recently as 2006 suggest that DHSVM subsurface flow algorithms route water to all eight neighboring cells (Wigmosta *et al*., 1994; 2002; Wigmosta and Perkins, 2001; Doten *et al.*, 2006). In addition, several diagrammatic representations of model processes shown in these articles and on the DHSVM website indicate this eight-cell neighbor concept. But according to the model developers as stated in the frequently asked questions section of the DHSVM website, the ability to incorporate eight-neighbor flow has not yet been achieved successfully (DHSVM Administrator, 2006B). The code to support this approach was written; however, the eight-neighbor cell code has been commented out. The reason provided on the website is that eight-direction flow method was incompatible with the digital elevation model networks (DEMON; Costa-Cabral and Burges, 1994) approach used to compute surface and subsurface flow pathways in DHSVM. DHSVM in its current state is capable of routing water and sediment in each of only four directions. Enabling eight-neighbor flow would require significant editing to the existing code. A more detailed description of the individual modules within the main DHSVM follows.

1.6.1 ***Evapotranspiration***. DHSVM uses a two-layer vegetation input to represent the canopy and understory. Accurate representation of the vegetation is important with respect to evapotranspiration calculations because vegetation presence

and structure influence the temperature, moisture, wind, and radiation regimes of both the air and soil (Campbell and Norman, 1989). Because DHSVM allows the user to parameterize any number of individual vegetation types, multi-cohort stands can be adequately described using this two-layer model. Evapotranspiration is modeled through step-wise calculations in order to ensure that the total evaporation from both vegetation layers does not exceed the rate of potential evaporation from the overstory layer. This approach also allows DHSVM to account for the presence and percent coverage of a canopy, the existence of wet and dry fractions within the overstory, the ability of any wet fraction to dry during a time step, and the presence of a ground snowpack and its effects on plant transpiration. When a snowpack is present, it is assumed to cover the entire grid cell; therefore, no evapotranspiration from the soil surface or understory is calculated while a snowpack exists on any grid cell. The partitioning of the vegetative layers into wet and dry fractions enables the model to account for interception, storage, and throughfall.

DHSVM first calculates evaporation from the wet fraction of the vegetation at the potential evaporation rate. If intercepted water remains at the end of the time step, then a Penman-Monteith approach models transpiration from dry vegetative surfaces. In the absence of an understory, evaporation from the upper soil layer is calculated as a function of the potential evaporation rate, the soil moisture content, soil type, and antecedent moisture conditions (Wigmosta *et al.*, 2002).

Wigmosta *et al.* (1994) describe the methods used to calculate canopy resistance. Values for both the understory and overstory are calculated separately as a function of stomatal resistance, leaf area index (LAI), a species dependent minimum resistance

factor, air temperature, vapor pressure deficit, photosynthetically active radiation flux, and soil moisture values (Dickinson *et al.*, 1993).

Storck (2000) describes the specifics of the methods used to model aerodynamic resistance through the overstory canopy. Three different wind profiles are calculated. These include the profiles above the overstory (from the reference height down to the roughness layer just above the canopy top), through the canopy, and through the region comprised of the overstory trunk space. Aerodynamic resistance for the understory, soil, or snow surface is also calculated according to Storck (2000), and is a function of the displacement height of wind measurements and the roughness height of the surface over which the measurements are taken.

DHSVM calculates independent radiation budgets for both shortwave and longwave radiation for the overstory, the understory, and the soil surface. The overstory receives incident shortwave radiation. The understory below an existing overstory receives attenuated shortwave radiation and exposed understory receives direct shortwave radiation. The exchange of longwave radiation takes place between the overstory and the sky, between the overstory and the understory, and between the understory and the ground (Wigmosta, 2002).

1.6.2 *Two-Layer Ground Snowpack Model*. DHSVM models the processes associated with snowpack morphology as described by Storck and Lettenmaier (1999; 2000) and Storck (2000) using a two-layer ground snowpack representation of snow accumulation and melt. This snowpack model utilizes separate energy and mass balance components to represent the various physical processes affecting the snowpack. It also accounts for energy exchanges taking place between the atmosphere, overstory canopy,

and main snowpack. The energy balance components of the model address snowmelt, refreezing, and changes in snowpack heat content, while the mass-balance equations address the snow accumulation and ablation processes, transformations in the snow water equivalent, and snowpack water yield (Wigmosta, 2002).

DHSVM represents the two-layer snowpack as a thin surface layer and a main pack layer. Calculations of net radiation and energy fluxes take place only for the surface pack layer. Albedo of the snow surface affects the radiation budget. An exponential function based on the number of days since the last snow accounts for the decay of the snow surface albedo (Laramie and Schaake, 1972). Sensible heat flux is calculated for the surface snow layer as a function of aerodynamic resistance, air temperature, snow surface temperature, and snow density. The model uses the bulk Richardson's number to correct aerodynamic resistance for atmospheric stability (Anderson, 1976). The net energy exchange for the snow surface layer determines the amount of available energy to refreeze water or melt existing snow. If this energy balance is negative, then any liquid water present may be refrozen. If it is positive, and the cold content of the snowpack has been satisfied, then this excess energy will begin to produce snowmelt (Storck and Lettenmaier, 2000).

Additional mass is added to the snowpack in both liquid and solid phases, and the delivery of this water is affected by the presence of an overstory. Snow delivered to the surface layer accumulates until the width of snow exceeds a defined maximum thickness threshold. At that time, excess snow and its associated cold content is transferred to the pack layer. Liquid water in excess of the liquid water holding capacity of the surface layer drains into the pack layer. Snowpack temperature determines whether that volume

of water will refreeze or whether it will be routed to the soil as snow outflow (Wigmosta *et al.*, 2002).

1.6.3 ***Canopy Snow Interception and Release.*** DHSVM simulates canopy snow interception and release via a one-layer mass and energy balance model (Storck and Lettenmaier, 1999; 2000; Storck, 2000). This snowpack model explicitly accounts for the topographic and vegetative influences on the energy and mass exchanges taking place on the snow surface (Wigmosta *et al.*, 2002), specifically the processes governing snow interception, sublimation, mass release, and melt from a forest canopy.

DHSVM partitions precipitation into rain and snow based on atmospheric temperature per pixel and time step, and according to user defined minimum and maximum temperatures for rain and snow occurrence. A step-wise calculation dictates snow interception patterns. The volume of intercepted snow is determined by the maximum interception storage value. This is directly correlated to the leaf area ratio of each pixel and is based on field observations by Storck (2000). Snow in the canopy may subsequently intercept rainfall up to its water holding capacity. Bare branches of deciduous vegetation types may also intercept rain. Excess rainfall becomes canopy throughfall.

Snowmelt from intercepted canopy snow is calculated similarly to ground snowpack melt, utilizing a modified energy balance approach for each time step. As the snow in the canopy melts, it is converted into liquid canopy water until the water holding capacity of the canopy snowpack is met. Snowmelt in excess of this value results in meltwater drip. Mass release of canopy snow is linearly related to meltwater drip in DHSVM. If sufficient snow is available in the canopy, and sufficient meltwater drip is occurring, then

mass release of the canopy snow occurs for that pixel (Storck, 2000; Wigmosta *et al.*, 2002).

1.6.4 ***Unsaturated Soil Moisture Movement.*** Movement of water through an unsaturated multi-layer soil profile is represented dynamically in DHSVM, as described by Wigmosta *et al.* (1994). Water is delivered to the soil surface by way of the mechanisms of throughfall, snowmelt, or surface runoff from adjacent cells. DHSVM calculates infiltration into the upper soil layer based on the maximum infiltration rate defined by the user. Any water in excess of the infiltration capacity is then managed by the surface routing components of the model. Water that has infiltrated into the unsaturated soil profile percolates through the additional layers according to Darcy's Law. A unit hydraulic gradient calculated according to the Brooks-Corey relationship is used to calculate hydraulic conductivity (Brooks and Corey, 1964). This relationship describes the portion of the water-retention curve only for pressures at which air will enter the soil. The Brooks-Corey hydraulic conductivity equation is:

$$\frac{K(\theta)}{K_s} = \left[\frac{(\theta - \theta_r)^n}{(\phi - \theta_r)} \right] \qquad \textbf{(1)}$$

where $K(\theta)$ is the hydraulic conductivity for a given water content (cm/h), K_s is the fully saturated hydraulic conductivity (cm/h), θ is the volumetric water content, θ_r is the residual water content, ϕ is the total porosity, and n = [3 + (2/ pore-size distribution)] (Maidment, 1993).

Water may be removed from the unsaturated profile via three pathways. First, evapotranspiration may take place from the upper soil layer. Transpiration also occurs from within the soil profile according to the total percent of plant roots in a soil layer for

both vegetation layers. Finally, desorption from the top soil layer may occur and is calculated for every time step as a function of the potential evaporation demand at the soil surface and the soil desorptivity.

DHSVM first calculates infiltration into the upper layer. Next, the calculations address the downward vertical moisture transfer moving from top to bottom through the soil profile. The net flux of any lateral flow is added to the bottom layer. The model then calculates soil moisture in a step-wise fashion as it moves up through the individual layers of the soil profile. If the moisture exceeds the porosity for an individual layer, then the moisture is set equal to the porosity. If the calculated soil moisture is less than the porosity value, then that available water is added to the overlying layer until the uppermost soil layer is reached.

1.6.5 ***Saturated Subsurface Flow*****.** DHSVM routes saturated subsurface flow downslope using both a kinematic and a diffusion approach. The kinematic method uses slopes to approximate the hydraulic gradient for those cells representing steep areas with thin, permeable soils. In contrast, the diffusion assumption approximates hydraulic gradients using local water table slopes, specifically for areas of low vertical relief (Wigmosta and Lettenmaier, 1999; Wigmosta *et al.*, 2002).

The rate of subsurface flow per time step is calculated for each pixel and in each of four directions. Saturated subsurface water movement is controlled in DHSVM by the transmissivity of an individual grid cell, as determined by the lateral saturated hydraulic conductivity of the soil profile. This value is assumed to decrease exponentially with depth, according to a user-defined exponential decay coefficient. Exponential decay coefficient values typically range from 1.0 – 3.0. Subsurface water moving downslope

may be intercepted by either a road or a stream segment. In the case of the road segment, interception occurs when a road cut depth exceeds the depth to the water table. Stream interception occurs similarly. When the water table rises above a streambed, that water is intercepted by the channel (Wigmosta *et al.*, 2002).

1.6.6 *Surface Overland Flow.* Overland flow is uncommon in undisturbed forests of western Montana, but the occurrence of this flow mechanism may be more widespread following forest fire (Ward and Elliot, 1995). DHSVM addresses this physical process on a per pixel basis. Generation of overland flow occurs when at least one of three physical conditions is met. First, overland flow occurs when the sum of throughfall and snowmelt exceeds the user-defined infiltration capacity of the soil. Surface flow may also be generated if throughfall or snowmelt occurs for a cell that already represents a fully saturated soil layer. Finally, return flow from a water table rising above the soil surface will generate surface water for routing in DHSVM (Wigmosta *et al.*, 1994; Wigmosta *et al.*, 2002).

Surface water is routed on a cell-by-cell basis downslope in a similar fashion to subsurface routing. Fundamentally, the overland flow algorithms account for cell size, the volume of the surface water, the time step, and the amount of water leaving the system via culvert outflow (Wigmosta *et al.*, 2002).

1.6.7 *Channel Flow.* DHSVM routes flow through the network of road ditches and stream channels using a cascade of linear channel reservoirs. Preprocessing of the road and stream networks allows the model user to assign hydraulic properties to individual road or stream classes, including length, width, depth, roughness, and channel slope. Each channel segment represented in the model has uniform hydraulic properties.

These constants imply a uniform flow velocity per channel segment and time step (Wigmosta *et al.*, 2002).

Water is delivered to a channel via culvert outflow, subsurface contributions of lateral inflow, and direct delivery by way of overland flow. Once it is in the channel system, water remains in the system. It is passed segment by segment until it reaches the watershed outlet. The only way water is removed from a channel is via delivery directly back to the land surface by way of a culvert. This water is then available again for surface runoff or infiltration routing (Wigmosta *et al.*, 1994; Wigmosta *et al.*, 2002).

1.6.8. DHSVM Fire Model Description. The DHSVM fire model as described by Lanini (2005) incorporates code changes that enable the model to integrate fire as a disturbance into hydrologic simulations. Unlike DHSVM version 2.0.1, the soil and vegetation inputs into the DHSVM fire model are not static. Based on the user-defined date of a fire and a vegetation burn severity grid at the same resolution and extent of the other raster inputs, the DHSVM fire model edits the soil and vegetation parameters to reflect the burn severity patterns following a fire. The fire model creates new soil and vegetation types characterized by the pre-fire conditions and the associated burn severity classification. In addition, the model allows soil and vegetation to recover following a fire, making yearly adjustments to the physical parameters of fire-affected pixels.

The fire model addresses vegetation mortality and regeneration through adjustments made to the values describing the vegetation type classification, LAI, root cohesion, and vegetative surcharge. Vegetative surcharge is a factor related to the weight of vegetation on a slope and the relationship of this weight to slope failure probabilities. The root cohesion and vegetative surcharge components address the effects of fire on soil erosion

and hillslope failures, and as such, these parameters are only incorporated when the optional sediment routing and mass wasting modules are utilized by the modeler. The changes in the vegetation type and LAI values following the fire affect the water and energy balances in the main DHSVM code. LAI recovery follows sigmoidal and logarithmic relationships internally described in the fire model code, and the LAI values are assumed to recover completely in 10-yrs, regardless of the burn severity (Lanini, 2005). The DHSVM fire model also represents soil hydrophobicity following fire through adjustments made to vertical infiltration capacity of those soils corresponding to high severity burns and resinous vegetation types.

A unique advantage of the fire model is that it internally accounts for the recovery of the landscape following fire, allowing the vegetation and soil to eventually return to the pre-fire conditions. This factor is particularly beneficial for long-term simulations, such as those presented by Lanini (2005). In addition, the fire model allows for simulation of watershed hydrology for pre- and post-fire conditions during the same model run. This is in contrast to DHSVM version 2.0.1, which requires a separate model run for every different simulated landscape scenario. From this perspective, the DHSVM fire model may provide increased overall efficiency and considerable time savings. Despite these advantages, because the DHSVM fire model is still in its infancy, thorough documentation detailing the internal processes driving the model is nonexistent. While this tool holds promise from both research and management perspectives, simulations produced must be considered preliminary until the documentation describing the code logic is produced.

2. OBJECTIVES

2.1 ***MODEL SELECTION JUSTIFICATION.*** DHSVM holds research interest for many reasons. The first and most attractive feature of DHSVM from a research perspective is that it is a physically-based, fully-distributed model. The distributed nature addresses the spatial variability of landscape features and meteorological conditions presented by mountainous, forested terrain. In addition, because it is physically-based, there is theoretically little need for model calibration. This extends the potential research utility of DHSVM to ungaged catchments. The level of detail found in the multi-layer canopy, soil, wind profile, and snowpack representations used in DHSVM is superior to the landscape representations in other widely used hydrologic models. This level of detail should hypothetically enhance DHSVM's ability to address the actual physical processes driving the hydrologic cycle at the watershed scale.

Another essential feature for watershed scale modeling in these types of landscapes is the ability of the model to operate at sub-daily iterations. DHSVM calculates the full water and energy balance for every pixel and for every time step. This level of complexity is necessary to capture the highly dynamic processes affecting snow accumulation and ablation in a snow-dominated system.

The model design also lends itself to incorporation of a wide variety of spatial data types. While the inputs are extensive, they are also somewhat flexible. The appeal lies in the adaptability of the model. The user defines the spatial and temporal resolution of DHSVM based on the data available for the particular research application. Distributed spatial data gathered through remote sensing technologies and geostatistical interpolations of point field measurements could both be integrated into a DHSVM

simulation. Other types of landscape models may be used to simulate the necessary meteorological parameters used to drive a DHSVM simulation when point metrics are unavailable for a particular watershed.

Finally, DHSVM holds promise as a potential management tool. The preprocessing of the spatial inputs required by DHSVM is time consuming; however, once the data are collected and formatted for a geographic area, and the model is compiled and running on a specific computer system, then the ease of use is relatively high. The extensive list of output options, as well as the availability of associated erosion, mass wasting, and sediment routing modules, all present the potential for a wide range of management applications involving the simulation of hydrologic processes at a watershed scale.

2.2 *MODEL LIMITATIONS*. Increased model complexity, such as that provided by DHVSM, comes with both potential benefits and correlated drawbacks. The most significant issue with DHSVM is related to ease of implementation. Because DHSVM is a "research model," there is no user support beyond a web page and a user email list serve. This lack of support can be problematic for new model users for many reasons. First, the error reporting provided by the model code is relatively unspecific. New users, unfamiliar with individual error messages, must invest considerable amounts of time searching for the source of the unknown errors. In addition, implementation of DHSVM requires significant computer skills on the part of the modeler, including general knowledge of the Arc Macro Language (AML) used in GIS preprocessing steps, Linux platforms, and the C programming language. Knowledge in all of these areas is required to troubleshoot any unspecific errors produced by DHSVM. Finally, the model code has limited translatability between computers. Compiling all components of the code on a

modeler's unique computer workstation inevitably involves error troubleshooting and some editing of the internal model code. As more time has been invested by model developers to add new scientific components to DHSVM, less time has been used to streamline the model processes and code, thus introducing more potential sources of error and decreasing the translatability between machines.

The other significant issue of DHSVM involves the relationship between the cost of implementation versus the benefits of the simulations. The cost of using DHSVM is relatively high when compared to other hydrologic models. The utility issues described above, combined with the extensive list of high resolution spatial and temporal data, both demand a high level of effort on the part of the modeler to implement DHSVM. In contrast, the simulations produced through the calculations of full water and energy balances per pixel and time-step are only as good as the data used to drive the model. Overly coarse data inputs, whether they be characterizations of the landscape or the weather, will negate the alleged benefits provided by the spatially explicit nature of DHSVM.

2.3 ***PAST DHSVM APPLICATIONS.*** DHSVM has been predominantly used to model managed forested watersheds in western Washington affected by road building and forest harvests. It has been applied to catchments up to 10^4-km^2 in size, at resolutions ranging from 10- to 100-m, at sub-daily time steps ranging from 1- to 6-hours, and for multi-year simulations (DHSVM Administrator, 2006A).

Currently, there are only a few known applications of DHSVM focused on quantifying the impacts of forest fire on the hydrologic regime of a watershed. Putz *et al.* (2003) used DHSVM to predict the impacts of wildfire on the quantity and quality of

runoff on the Boreal Plain in Canada. Doten and Lettenmaier (2004), Lanini (2005), and Doten *et al.* (2006) describe the use of DHSVM to simulate sediment erosion and hillslope failures following forest fire on the east slopes of the Cascade Range in central Washington. Lastly, Tangedahl (2006) applied DHSVM to the Copper Creek watershed in western Montana following the Snow Talon Fire. His research focused on implementation of the DHSVM fire model and the optional Mass Wasting Module.

2.4 *THESIS STATEMENT.* This research will utilize DHSVM to assess the cumulative effects of a high intensity forest fire on the hydrology of a mountainous, forested, snow-dominated catchment in western Montana. The purpose of this work is primarily to assess the ability of DHSVM to simulate runoff in these types of variable systems following forest fire. Secondary benefits of this research will include expanding the body of knowledge regarding DHSVM applicability and use, as well as providing an assessment of the spatial limits of this model by applying it to a new and unique setting. Three specific research goals will be addressed, including:

1. model calibration utilizing historical stream gage records and cited physical values for soil and vegetation characteristics;
2. model validation involving the application of both the calibrated DHSVM version 2.0.1 and the DHSVM fire model to the burned Eightmile Creek watershed;
3. model version comparison involving statistical analysis and goodness-of-fit assessments of post-fire simulations produced with both DHSVM version 2.0.1 and the DHSVM fire model.

3. WATERSHED CHARACTERIZATION

3.1 ***GENERAL OVERVIEW*****.** The watershed of interest includes the area of land that drains into the Eightmile Creek tributary of the Bitterroot River, which originates on the west central slopes of the Sapphire Mountains in western Montana (Figure 1). The total drainage basin area is 72.3-km^2, and Eightmile Creek is a 4th order stream. The upper portion of the watershed is steep and forested and is owned and managed predominantly by the Plum Creek Timber Company. Gently sloping grasslands and human development surrounding the town of Florence characterize the remaining watershed area.

Figure 1 – ***Location of Eightmile Creek in western Montana*****.**

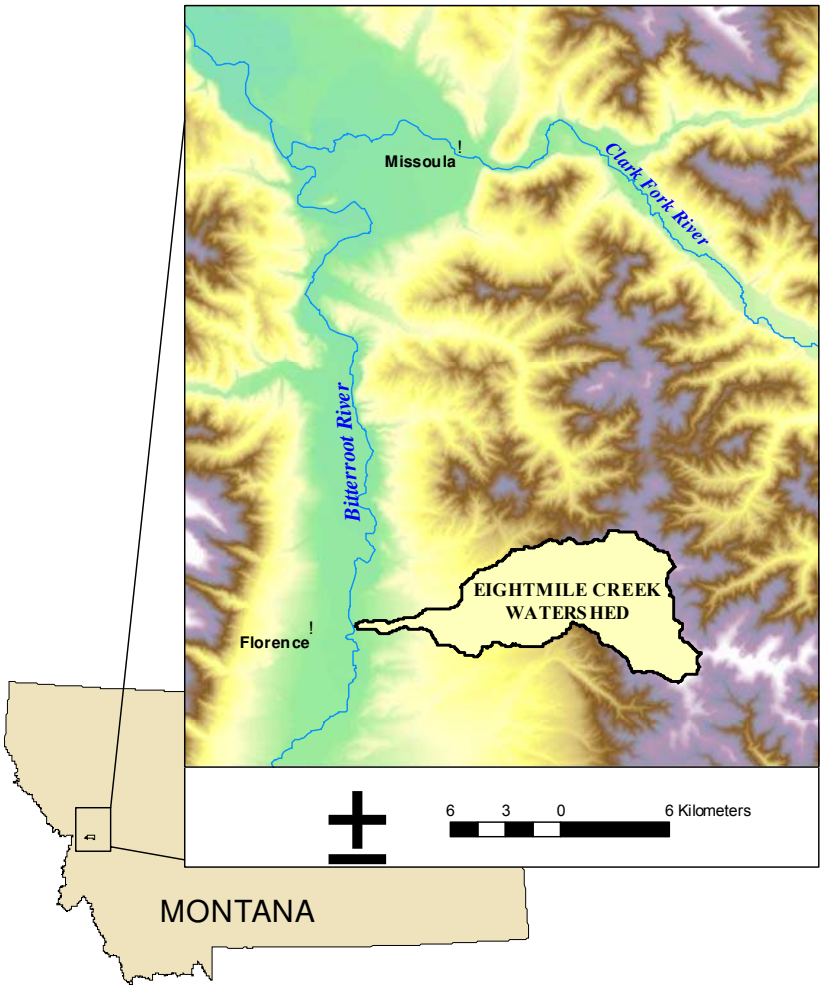

The lower watershed area was not of interest to this model application for three reasons: 1) DHSVM routing algorithms do not work in urban settings; 2) the research focus here is on forested, mountainous systems; and, 3) an historic United States Geological Survey (USGS) stream gage upstream served as a more logical point for watershed delineation. The ArcHydro application for ArcGIS 9.x (version 1.1) was utilized to delineate the catchment of interest from within the larger Eightmile Creek watershed. The result is a smaller drainage basin, representing 54.1-km^2 of forested area. Any future references in this thesis to the Eightmile Creek watershed will be referring to this upper catchment portion as displayed in Figure 2.

Figure 2 – ***Research watershed shown within the larger Eightmile Creek watershed, delineated from the location of an historic USGS stream gage.***

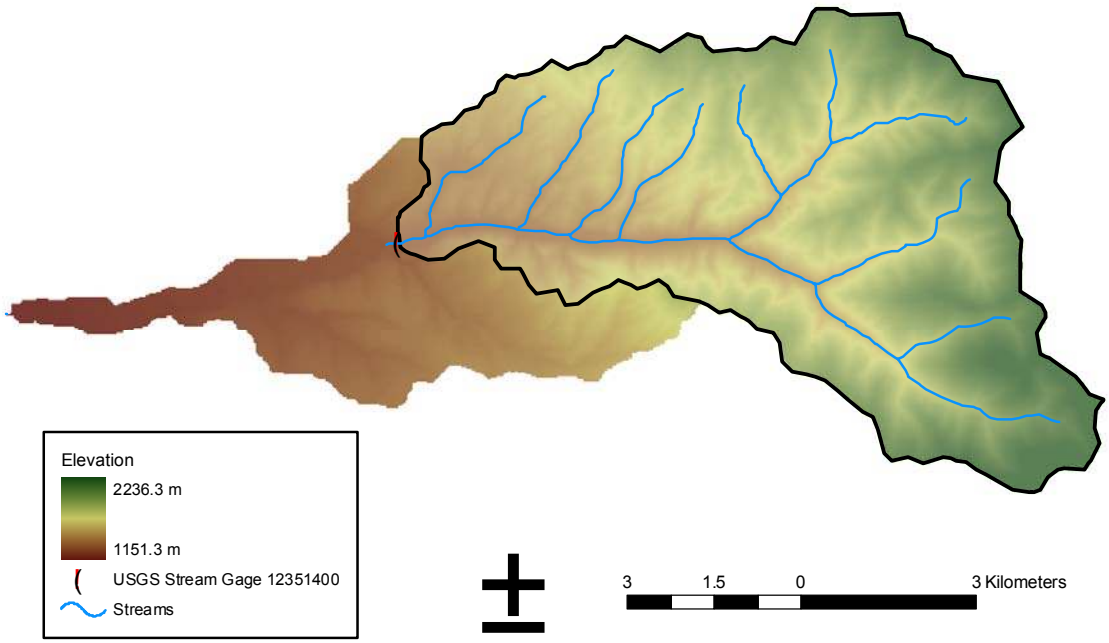

3.2 *TOPOGRAPHY.* Elevations in the study area range from approximately 1150-m (3773.0-ft) at the historic gauging station, to 2235-m (7332.7-ft) at the highest ridge. Steep mountain slopes characterize the watershed. Approximately 75% of the watershed area has a slope of greater than 15 degrees, with only 2% of the area characterized as flat (slopes less than 5 degrees). The mean slope value is 21 degrees. Figure 3 illustrates the incised drainage network where most of the steeply sloped areas are located directly adjacent to the channels. Slopes are categorized into general steepness categories according to Ramakrishna (2003) on the left, and a three dimensional viewpoint from the top of the southern watershed boundary, indicated by the red star, is shown on the right.

Figure 3 – *Eightmile Creek watershed slopes*. The map on the left shows the slopes displayed by general steepness category. The red star indicates the location of a northeast facing view, shown in three dimensions (right). The view shown is looking down into the northernmost stream drainage and further illustrates the steeply incised channel network and the generally rounded mountain peaks.

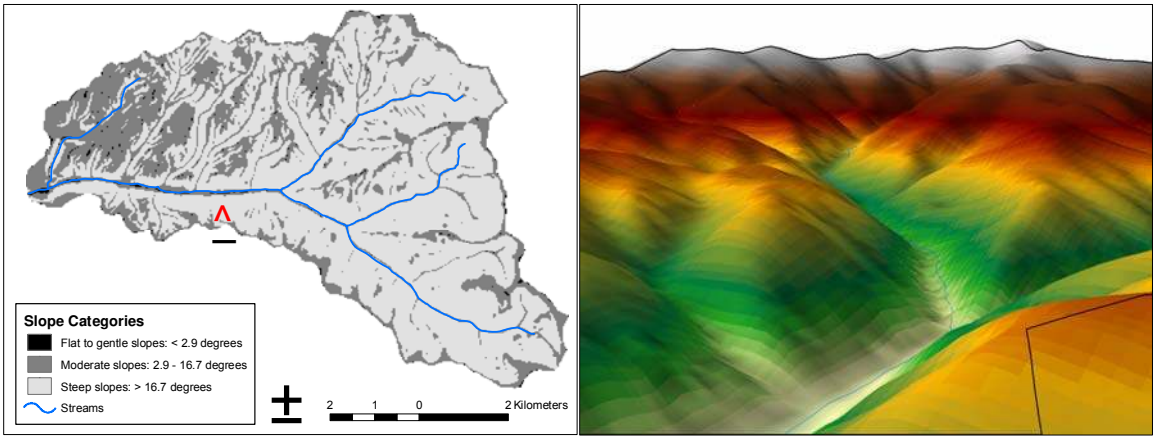

A hypsometric curve of the watershed provides an alternative representation of the nature of the terrain (Figure 4). This curve was constructed according to Strahler (1952) and shows the normalized elevation plotted against the normalized cumulative area. The

linear nature of the hypsometric curve for the Eightmile Creek watershed suggests evenly sloped terrain. Although it is generally very steep, this steepness tends to be consistently observed across the entire watershed area. As a result, constant temperature and precipitation lapse rates will likely serve as reasonable models of the orographic effects of elevation on these weather parameters.

Figure 4 – ***Eightmile Creek watershed hypsometric curve, after Strahler*** **(1952).**

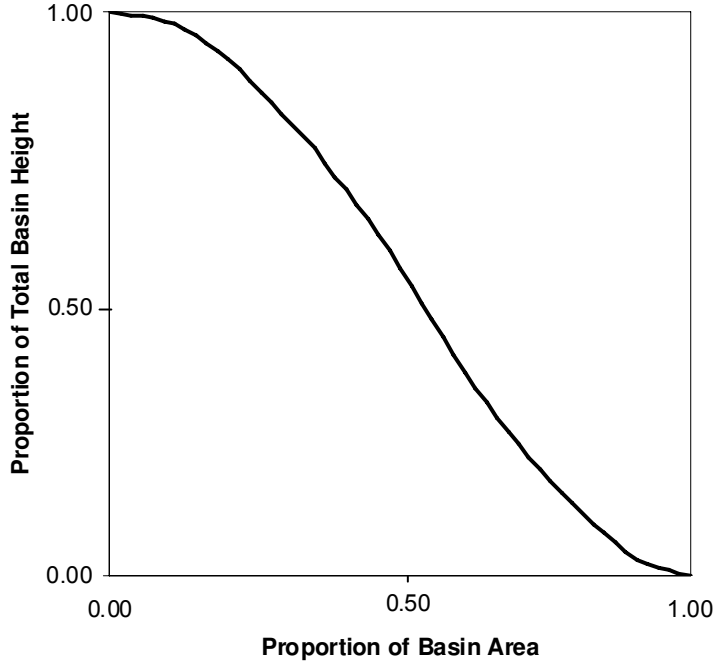

3.3 ***CLIMATE*****.** This is a snowmelt-dominated system with orographically driven weather patterns. Meteorological data from within the watershed boundaries are lacking. Approximate mean annual precipitation values, ranging from 35-cm at the lowest elevations to 90-cm at the highest elevations, were derived using the Forest Service Water Erosion Prediction Project's (FS WEPP) Rocky Mountain Climate Generator interface (Nicks and Gander, 1995). This tool utilizes the Parameter-Elevation

Regressions on Independent Slope Model (PRISM; Daly *et al.*, 1994) and historic meteorological data at point locations to predict monthly and annual average precipitations values for defined 2.5-minute grid cells.

3.4 *GEOLOGY.* Nearly 90% of the Eightmile Creek catchment is underlain by the Missoula Group Belt Series, a geologic formation of sedimentary rock from the Precambrian Era (Figure 5; Raines and Johnson, 1995). The rocks of the Belt Series are weakly metamorphosed siltstone dominated by argillites. The angular nature of this parent material tends to form soil profiles characterized by high internal shear strength (McClelland *et al.*, 1999).

Figure 5 – *Eightmile Creek watershed general geology map.*

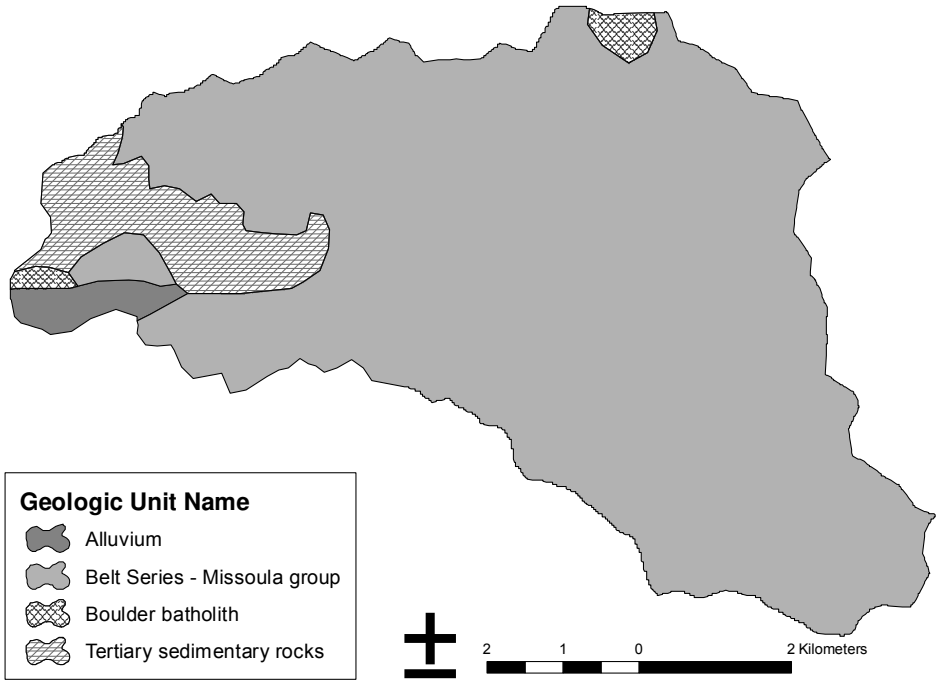

There are a few small zones (1.2% of the total watershed area) of localized geology distinguished by intrusive rocks from the Boulder batholith. The geology of the remainder of the drainage basin contains evidence of past glacial activity, as characterized by a finger of tertiary sedimentary rocks such as those found in ancient lakebeds, as well as a portion of unconsolidated alluvium near the mouth of the watershed that indicates past glacial drift (Raines and Johnson, 1995).

3.5 *SOILS*. The soils in the Eightmile catchment are inceptisols (Soil Survey Staff, 1999). The soils are all some variety of loam, most with high volume percentages of rock fragments. Gravels are the dominant coarse fragments found throughout the soil profiles. Eightmile soils are generally characterized texturally as moderately coarse to medium textured soils dominated by gravels (Soil Survey Staff, 1994). They may be further grouped into three general textural classes, including gravelly loam, gravelly silt loam, and gravelly sandy loam (Soil Survey Staff, 1994; 2006).

3.6 *VEGETATION*. The Eightmile Creek watershed is a working forest, and the legacy of harvest practices is evident in the vegetation found throughout the drainage basin. The vast majority of the pre-fire vegetation was evergreen coniferous forest, composed primarily of Douglas fir (*Pseudotsuga menziesii*) and ponderosa pine (*Pinus ponderosa*). Patchy areas of low cover resulting from harvest practices were found throughout the watershed, including grassy areas, bare ground, and shrublands of various densities. Naturally formed grasslands could be seen near the watershed outlet where the steep mountain slopes begin to transition to the Bitterroot River floodplain. The main riparian corridor was generally dense with deciduous shrubs and trees, and some sporadic pockets of western larch (*Larix occidentalis*) were found in the higher elevations.

3.7 *ROADS*. The Eightmile Creek watershed has an extensive forest road network consisting primarily of dirt roads in various states of use and disrepair. There are approximately 220-km of road in the upper catchment portion, with a road density equal to approximately 4.34-km of road for every square kilometer of land (Figure 5). Many of the roads are spur or jammer roads related to forest harvest practices (Woods, 2005).

Figure 6 – *Eightmile Creek watershed forest road network map*.

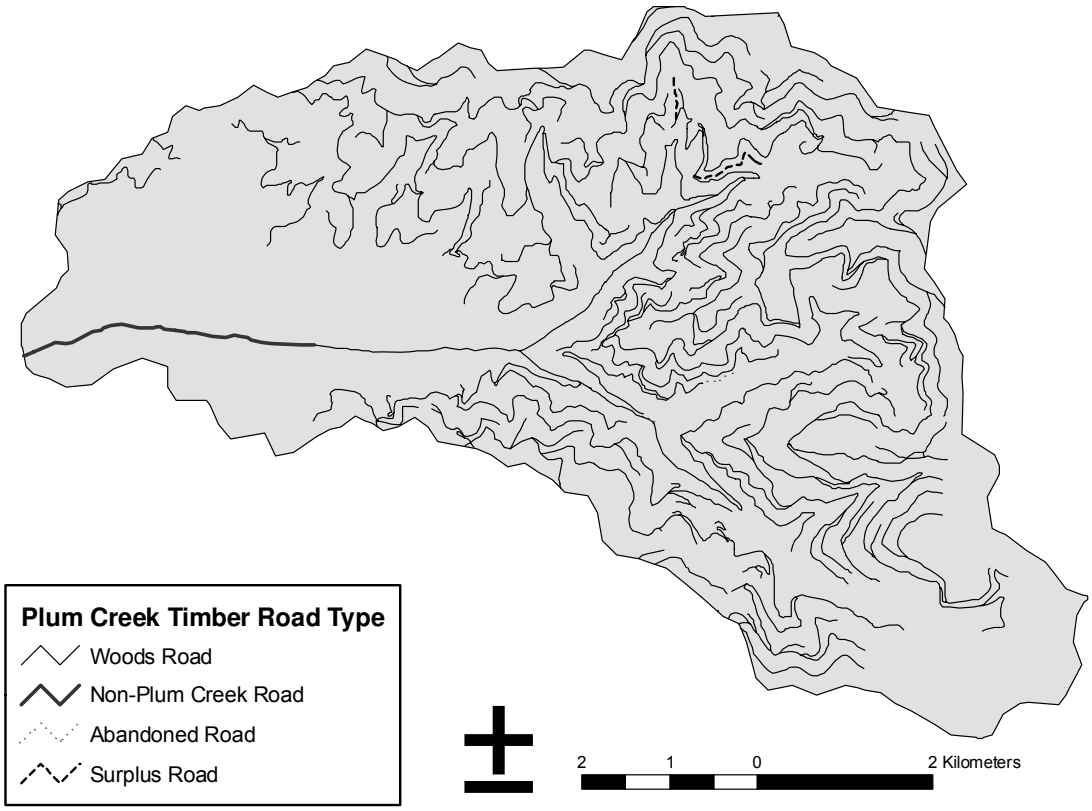

3.8 *STREAMS*. Digital stream data were obtained from the High Resolution National Hydrography Dataset (United States Geological Survey and United States Environmental Protection Agency, 2000; Figure 7). According to these data, the Eightmile Creek watershed has a drainage density of approximately 1.1 km/km^2.

Drainage density values in steep terrain are affected, in part, by the slope stability, and densities tend to be highest in watersheds with non-resistant lithologies (Wohl, 2000). Thus, the low drainage density value of the Eightmile Creek catchment may reflect the stable lithology of the area.

Figure 7 – ***Eightmile Creek watershed stream network map*****.**

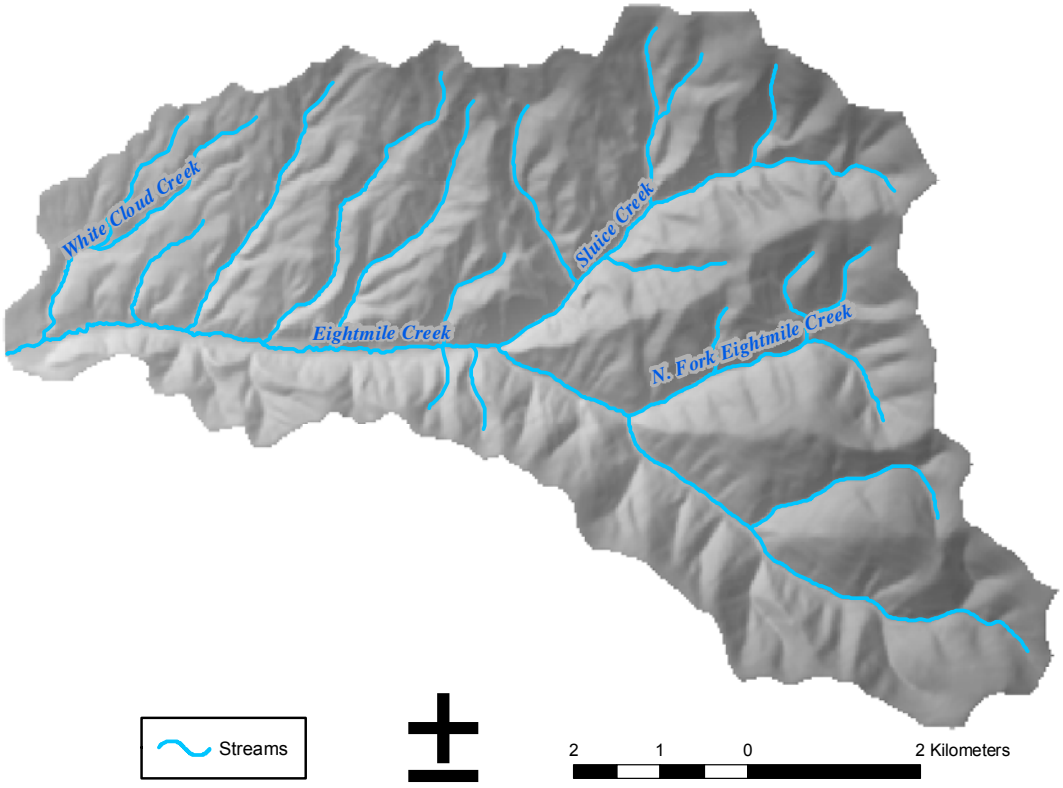

3.9 *COONEY RIDGE FIRE COMPLEX*. On August 8, 2003, multiple lightning strikes sparked a fire in the Cooney Ridge area, approximately 11-mi east of Florence, Montana, in Missoula County. The Cooney Ridge Fire Complex burned for over a month. The fire was ultimately contained September 14, and the final acreage burned was estimated at 26,100-acres (105.6-km^2; Figure 8).

Figure 8 – *Cooney Ridge Fire Complex perimeter relative to the Eightmile Creek watershed* (Lolo Burned Area Emergency Recovery Team, 2003).

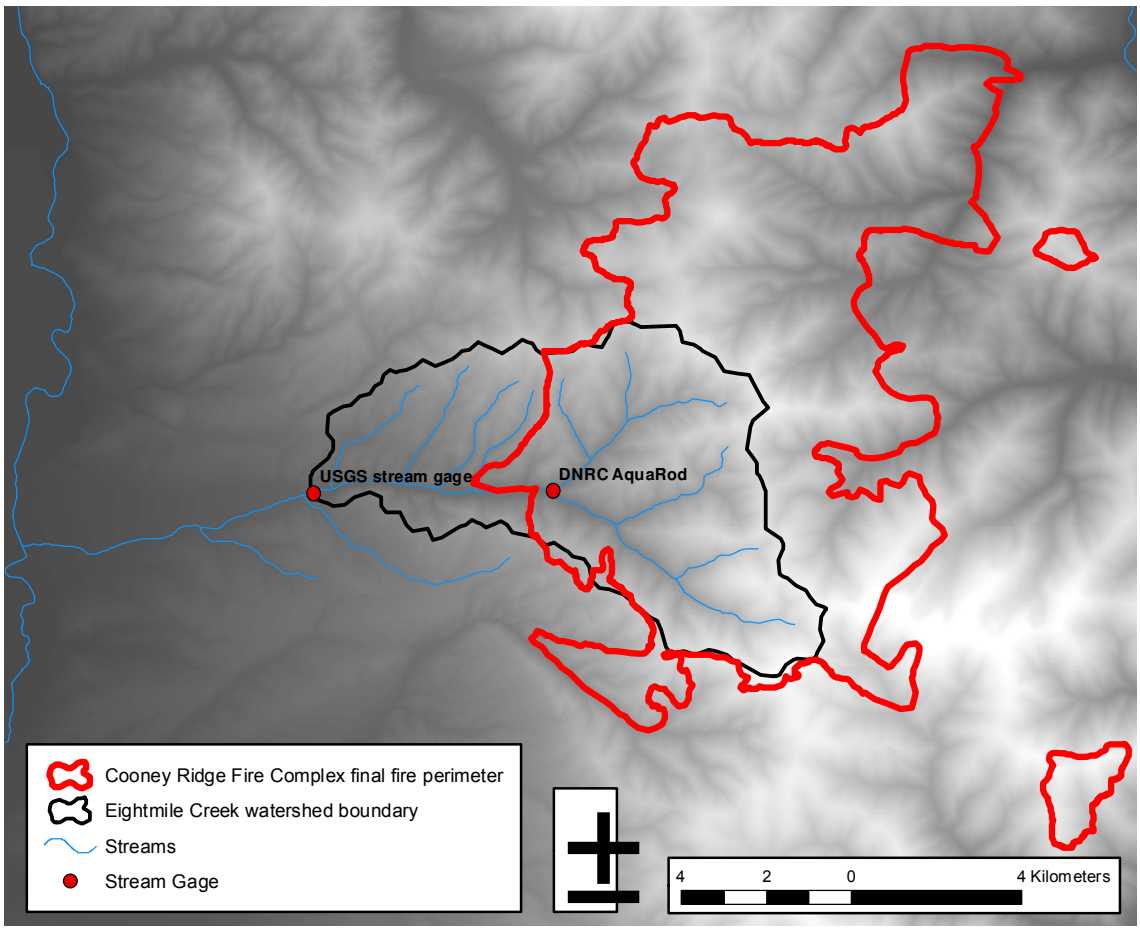

The Eightmile Creek watershed was hit especially hard by this fire. Over 50% of upper watershed area burned, and most of the fire severity observed with respect to the vegetation was high (Figure 9). Soil burn severity was characterized as low throughout the affected area (Lolo Burned Area Emergency Recovery Team, 2003). This soil burn severity assessment contradicts personal and anecdotal field observations of the burned landscape following the fire. A fire-wide classification of low soil burn severity seems overly coarse and potentially inaccurate for some of the hardest hit areas.

Figure 9 – ***Cooney Ridge Fire Complex burn severity map within the Eightmile Creek watershed*** **(Lolo Burned Area Emergency Recovery Team, 2003).**

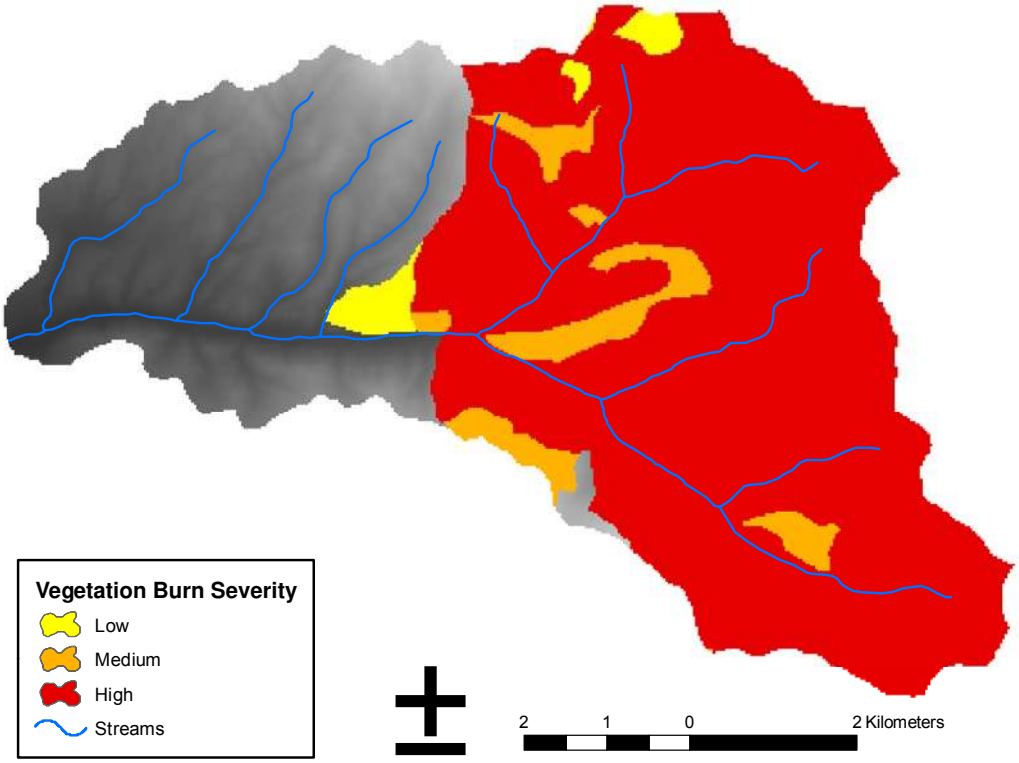

A Forest Service Burned Area Emergency Response (BAER) Team conducted a resource assessment immediately following the fire. In the Eightmile Creek drainage basin, the resources of greatest concern included the soil and water resources threatened by the extensive forest road network. Assessment of the road system found significant hazards associated with the erosion and mass wasting potential following the fire. Specific threats identified involved the intersections of temporary harvest roads and steep ephemeral headwater watersheds (Lolo Burned Area Emergency Response Team, 2003; Figure 10).

Figure 10 – ***Post-fire erosion hazards associated with an extensive forest road network, steep slopes, and high severity fire*** **(Lolo Burned Area Emergency Recovery Team, 2003).**

4. METHODS

DHSVM version 2.0.1 was calibrated to the Eightmile Creek watershed using recorded streamflow data taken for the 1958 – 1963 water years. Following model calibration, DHSVM was used to simulate Eightmile Creek streamflow in the aftermath of a near catchment-wide stand-replacing forest fire. Utilizing post-fire streamflow data recorded during the 2004 – 2006 snowmelt seasons, the simulations produced by DHSVM version 2.0.1 in the post-fire landscape were compared to simulations produced by the DHSVM fire model in the same setting. The goal was to compare the performance of each model version with respect to modeling fire effects on hydrology in a forested drainage basin. Hence, the three main components of this research include model calibration, model validation, and model version comparison. The general progression of each of these components is visually outlined in Figure 11.

Figure 11 – *Research progression flowchart*. This schematic illustrates the general research progression addressing the three main areas of focus, including 1) calibration, 2) validation, and 3) version comparison.

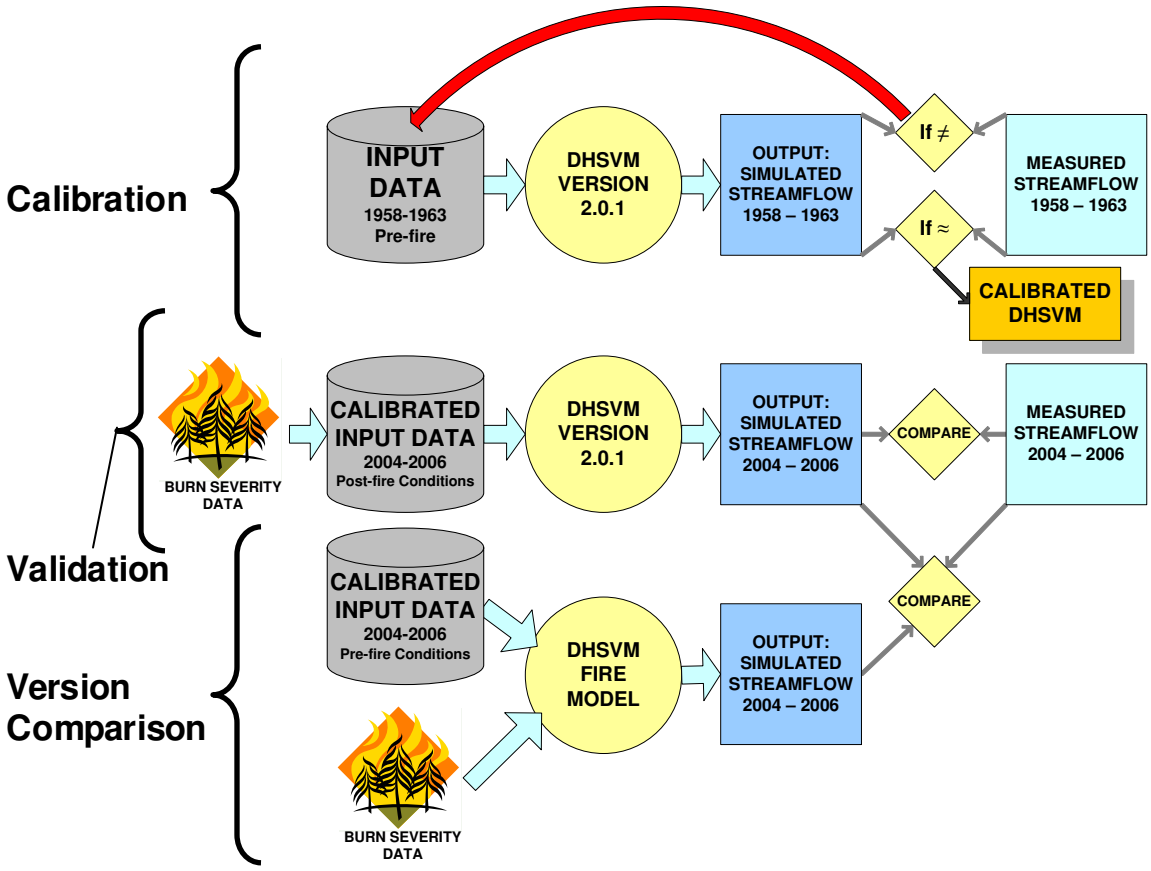

In addition to the three main areas of focus described above, there was a basic progression of preprocessing steps completed for each of the two periods of interest corresponding with available streamflow data and representation of pre- and post-fire watershed conditions. Implementation of DHSVM basically involves GIS preprocessing of the necessary spatial inputs, collection and formatting of meteorological drivers, formatting the necessary text files, and utilizing these three main input components to run the model (Figure 12). This same series of steps was completed for both the pre-fire data (calibration) and the post-fire data (validation and version comparison). This process,

related to each of the three main areas of focus (calibration, validation, and version comparison), is described in detail in the following sections.

Figure 12 – *Preprocessing schematic*. This figure illustrates the basic preprocessing steps needed to implement DHSVM for a specific time and location.

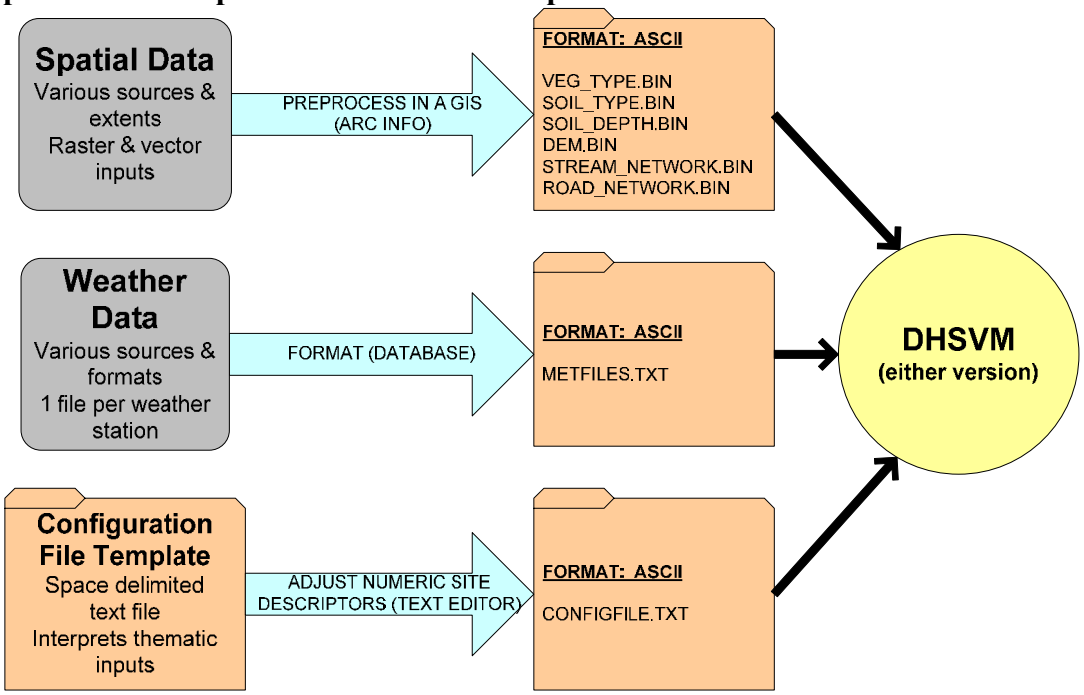

4.1 *GIS PREPROCESSING.* Spatial inputs into DHSVM were compiled, edited, and formatted using ArcGIS 9.1, specifically using ArcMap, ArcCatalog, and ArcInfo Workstation software. For each of the post-fire applications, soil and vegetation inputs were altered according to a grid of fire severity. The remaining spatial inputs, including grids of soil depth, elevation, and watershed extent, as well as the vector coverages of the stream and road networks, remained unchanged between the calibration and validation applications.

4.1.1 *Raster Inputs*. A seamless 30-m resolution digital elevation model was obtained for the Eightmile Creek watershed from the National Elevation Dataset (United

States Geological Survey, 2002). DHSVM is unable to handle sinks in the landscape, and a depressionless DEM is required for the successful generation of a stream network. No known natural sinks occur in the steep upper portion of the Eightmile Creek drainage basin, therefore any sinks present are likely the result of slight errors in the DEM data. The input DEM was reconditioned in ArcMap in order to produce a depressionless DEM for hydrologic simulations. This reconditioning is a ArcHydro 1.1 process that enforces a linear drainage pattern onto the DEM grid. This is completed through two basic processes: 1) filling in sinks in the drainage area by raising the elevations of those grid cells, and 2) lowering the elevation of the cells corresponding with the vector drainage network, effectively burning the channel network into the DEM (Hellweger, 1997).

Soils spatial data were obtained online from the United States Department of Agriculture Natural Resources Conservation Service (USDA NRCS). The datasets used include the State Soil Geographic Database (STATSGO; Soil Survey Staff, 1994) and the Soil Survey Geographic Database (SSURGO; Soil Survey Staff, 2006). STATSGO soils data are at the resolution of 1:250,000. The more detailed SSURGO data provide soil information at a scale of 1:24,000; however, the digital coverage of the SSURGO data did not extend over the entire watershed area. These data only extend as far south as the Missoula-Ravalli County line, which runs in an east/west direction across the upper third of the watershed. This boundary is evident in the soil type input raster shown in Figure 13 on page 40.

In order to obtain the most detailed soil raster for input into DHSVM, the STATSGO and SSURGO grids were combined in ArcMap 9.1 using the Mosaic to New Raster Tool. These soil values were then generalized into three different dominant textural classes:

gravelly loam, gravelly silty loam, and gravelly sandy loam (Table 1). A soil profile as described by STATSGO and SSURGO that represents the majority of each of these textural classes in the watershed boundary was used to describe the soil properties in the DHSVM input file. These soil types are described in Table A2 in the Appendix.

Table 1 – ***Soil types represented in the Eightmile Creek watershed and used in the DHSVM input files*****.**

Dominant Soil Texture	Soil Database Source	Map Unit ID	Map Unit Name	% Watershed Area
Gravelly Loam	SSURGO	30B26	Wilde family, steep mountain slopes	37.8
Gravelly Silt Loam	STATSGO	MT57	Holloway gravelly silt loam, 30-60% slopes	55.7
Gravelly Sandy Loam	STATSGO	MT131	Winkler very gravelly sandy loam, 30-60% slopes	6.5

A soil depth grid is also a necessary spatial input. While the depth of the soil profile corresponding to specific soil types is generally known, this is not a readily available spatial data layer. DHSVM provides a script that generates a soil depth grid in ArcInfo for input into the model. This raster is created as a function of the watershed slope and a range of soil profile depths based on the soil type.

Vegetation cover data at the 30-m resolution were obtained online from the Satellite Imagery Land Cover (SILC) datasets (Fisher *et al.*, 1998). These data were derived using Landsat TM-5 imagery to classify vegetative cover for all of western Montana. This classification resulted in the representation of twenty-six different vegetation types within the Eightmile Creek watershed. This level of detail is not necessarily appropriate for DHSVM input, particularly because the data to accurately describe the differences in the physical parameters of this many different vegetation types are not available. Due to this

fact, the vegetation grid was reclassified into nine different classes using ArcMap. Tables A3 and A4 of the Appendix present the physical details of these different vegetation types, as well as the percent distribution by class.

To ensure that every pixel within the watershed of interest has a value associated with the elevation, soil type, soil depth, and vegetation type, DHSVM uses a mask of the watershed area to select only those cells within the watershed boundary for analysis (Figure 13). This process ensures that the extent of the area of interest is the same for every spatial input entered into the model. This raster is created using the ArcHydro Batch Watershed Delineation Tool. By working through a series of terrain preprocessing steps, each pixel in a DEM is assigned a flow direction. ArcHydro can then delineate a watershed polygon from any point specified within the raster by selecting all pixels that collectively drain to that point. The Eightmile Creek watershed shapefile was delineated using this ArcHydro tool. The ArcToolbox Feature to Raster Tool was then used to convert this polygon feature class to a 30-m resolution grid. Finally, this watershed mask raster was used in DHSVM to extract the Eightmile Creek drainage basin values from the soil type, soil depth, vegetation type, and DEM raster inputs.

Figure 13 – *DHSVM raster inputs*. Watershed mask is used to extract analysis pixels from input grids.

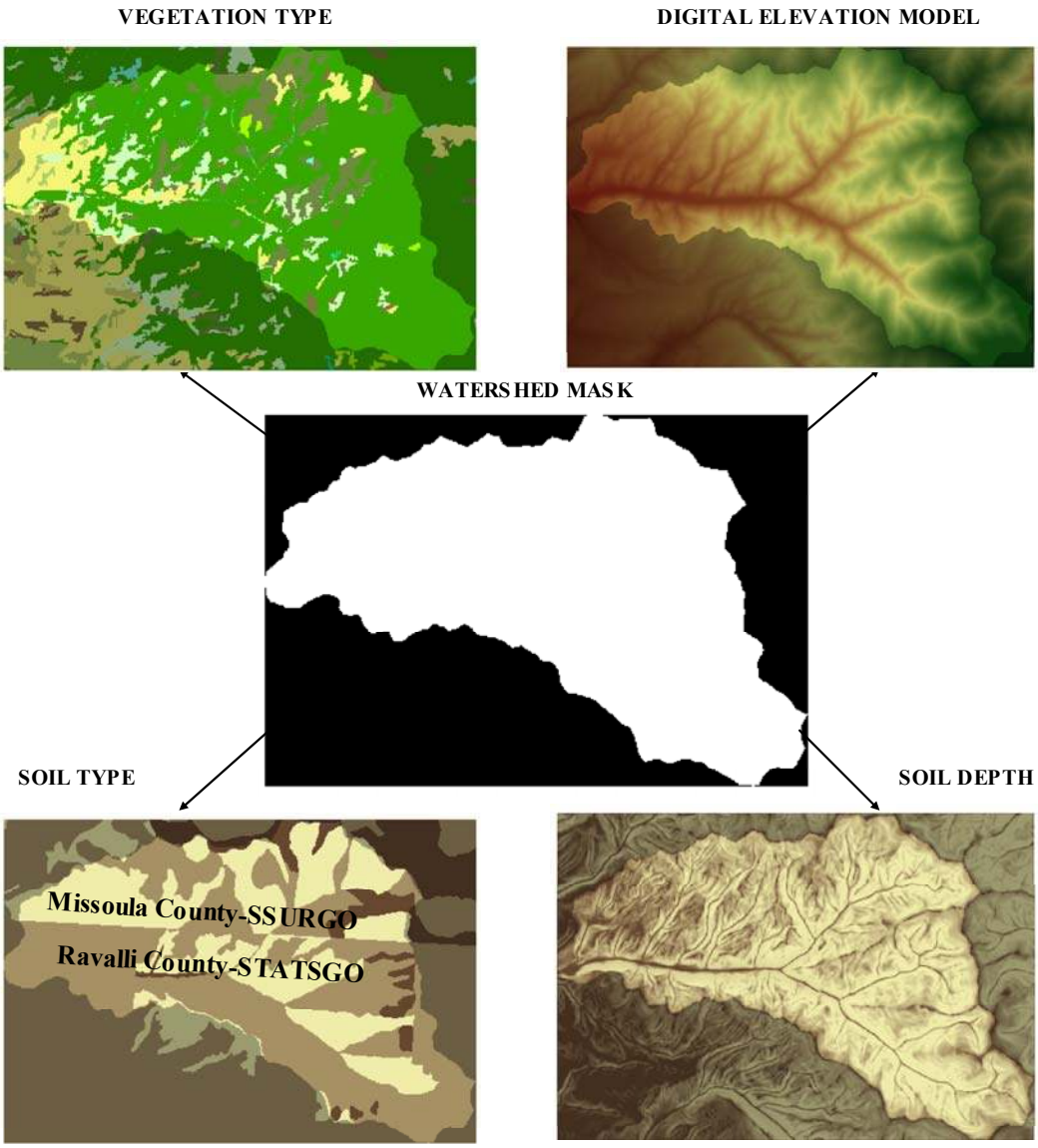

4.1.2 *Vector Inputs.* Road and stream networks are entered into DHSVM as coverages clipped to the watershed extent. Digital spatial data of the road network were provided by the Plum Creek Timber Company (Woods, 2005). Stream network data were obtained through the High-Resolution National Hydrography Dataset (United States

Geological Survey and United States Environmental Protection Agency, 2000). While these hydrology data provided a digital layer for mapping purposes, as well as the locations and identity of named stream reaches, they were not used as the stream coverage for input into DHSVM. Generation of a continuous stream network with assigned flow direction per segment is a necessary preprocessing step for implementation in DHSVM. The ArcHydro Stream Definition Tool creates a stream network with streamflow topology based on the reconditioned DEM, the watershed of interest as delineated in ArcHydro, and a stream initiation threshold defined by a specified number of pixels or area in km-^{2}. The contributing watershed area for stream initiation in the High-Resolution National Hydrography Dataset may be too low for proper routing of water in DHSVM. Storck *et al.* (1998) recommend a stream initiation level of 0.02-km^2 for small catchments on the west slopes of the Cascade Range in Washington. Doten and Lettenmaier (2004) used a larger stream initiation level of 0.04-km^2 for simulations on the drier east slopes of the Cascades. A drainage network was derived in ArcMap using ArcHydro at the 0.04-km^2 level for the Eightmile Creek watershed. Both the road system and the delineated drainage network coverages used for input into DHSVM are displayed in Figure 14.

Figure 14 – ***DHSVM vector coverage inputs including the road and stream networks*****.**

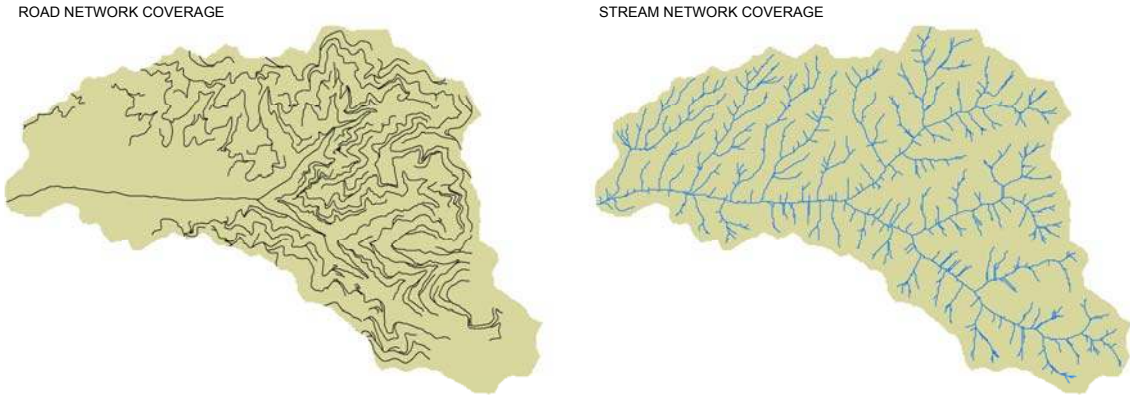

4.2 *METEOROLOGICAL INPUTS*. DHSVM may be run using meteorological records associated with point weather stations. If available, data from multiple stations can be incorporated into the model. DHSVM distributes weather parameters across the watershed of interest, for each model time step, using one of three user-selected interpolation methods. The model requires the following meteorological data for every time step and every weather station used: temperature (°C), wind speed (m/s), relative humidity (percentage), incoming shortwave radiation (W/m^2), incoming longwave radiation (W/m^2), and precipitation (m/time step).

Meteorological inputs were prepared separately for the calibration and validation applications. Meteorological records associated with Eightmile Creek are limited, particularly for the time coinciding with historical streamflow records (1957 – 1963). No weather data from within the watershed were available, and no high elevation meteorological data from any nearby catchments were available for the calibration period. In order to produce the most consistent analyses, it was necessary to use the same weather stations for both the model calibration and the post-fire simulations. The Missoula International Airport (MSO), at an elevation of 927.9-m and 31.6-km northwest of the watershed outlet was the only location where consistent meteorological data were available for both periods of modeling interest. MSO weather data were obtained from the National Climatic Data Center Online (National Oceanic and Atmospheric Administration, 2006). Remember that Eightmile Creek watershed elevations range from 1150- to 2235-m (Figure 2, page 24), and weather data from MSO represent lower elevation, valley-bottom climatic patterns, which are not necessarily representative of

weather patterns observed in the mountainous, higher elevations of the Eightmile Creek catchment.

4.2.1 ***Calibration Weather Generation*****.** The process used to generate the appropriate weather inputs was slightly different between the two simulation periods (pre- and post-fire watershed scenarios) due to the type of meteorological data recorded during each era. From 1957 to 1963, the weather data available online from MSO included daily recordings of minimum and maximum relative humidity, total precipitation, total snowfall, and minimum and maximum temperatures. In order to use this data to model 3-hr water and energy balances in DHSVM, it was necessary to distribute the daily values according to a general set of logic employing basic physical assumptions. First, daily minimum temperature values were assumed to occur at 6:00 A.M. and maximum temperatures were assumed to occur at 3:00 P.M. Next, daily minimum relative humidity measurements corresponded with the maximum daily recorded temperature (3:00 P.M.), and maximum relative humidity occurred during the coldest part of the day (6:00 A.M.). Constant lapse rates between each of these minimum and maximum values were used to assign unique temperature and relative humidity readings to each 3-hour interval. Daily precipitation recordings were assumed constant and daily totals were simply divided equally into eight, 3-hr increments. While these are relatively crude assumptions of naturally dynamic weather variability, a lack of availability of any sub-daily recordings make these general assumptions necessary.

Wind speed data were not available for MSO from 1957 to 1963. Historical monthly average wind speed values computed from hourly observations taken at MSO between 1992 and 2002 were used in place of these recordings (Western Regional Climate Center,

2002). These data, while general, are the best available wind speed data for MSO during the calibration period.

Both incoming shortwave and longwave radiation values are not parameters that all weather stations routinely measure and record, and MSO is no exception to this fact. These data were not available for either the calibration or post-fire period. The same methods were employed to generate these values for 3-hr increments, using available data, in both the pre- and post-fire simulation scenarios.

Incoming longwave radiation in the absence of cloud cover is essentially a function of the bulk atmospheric temperature and emissivity in accordance with the Stefan-Boltzmann law. Because neither of these properties fluctuates rapidly, incoming longwave radiation values experience essentially no diurnal variation (Oke, 1988). Nevertheless, individual 3-hr values of incoming longwave radiation were calculated according to empirical relationships using available recorded data. First, saturation vapor pressure, e_s (kPa), was calculated according to equation 1 (Ward and Elliot, 1995)

$$e_s = \exp\left[\frac{\left((16.78 \times T_a) - 116.9\right)}{T_a + 237.3}\right] \quad \textbf{(2)}$$

where T_a is the air temperature in degrees Celsius. Actual vapor pressure, e_d (kPa), was then calculated according to

$$e_d = e_s \times \left(\frac{RH}{100}\right) \quad \textbf{(3)}$$

where RH is the relative humidity in percent. Incoming longwave radiation values (L_{in}) in W/m^2 were calculated based on the following empirical formula (Brunt, 1932; Brutsaert, 1975),

$$L_{in} = \left[1.24 \times \left(\frac{10 \times e_d}{T_a + 273}\right)\right]^{\frac{1}{7}} \times \sigma \times (T_a + 273)^4 \quad \textbf{(4)}$$

where σ is the Stefan-Boltzmann constant, equal to 5.67 E-8 Wm^{-2} K^{-4}.

Devising the best methodology for determining the incoming solar radiation for each time step proved to be challenging. Incoming shortwave radiation values (S_{in}) correlating to the calibration period were not collected, and average shortwave radiation values were not available. Furthermore, because albedo, latitude, exposure, and vegetation cover and type all affect how solar radiation interacts with the Earth's surface (Jury and Horton, 2004), empirical equations to calculate incident solar radiation per time step utilizing routinely collected meteorological data do not exist. Tools are available that provide estimates of daily totals for incoming solar radiation. For example, the DAYMET model developed by the Numerical Terradynamic Simulation Group (NTSG) provides incoming shortwave radiation values at a 1-km resolution for 18-yrs of record (Thornton *et al.*, 1997; Thornton *et al.*, 2000; Thornton and Running, 1999). These values are calculated from measured temperature data according to a modified Bristow-Campbell equation (Bristow and Campbell, 1984),

$$T_t = A\left[1 - 0.9 * \exp\left(-B\Delta T^c\right)\right] \quad \textbf{(5)}$$

where T_t is the total transmission defined as the ratio between daily measured irradiance and daily extraterrestrial insolation (Thornton and Running, 1999). A, B, and C are empirical constants, and ΔT (°C) is the daily range of air temperature. However, the shortwave radiation values provided by the DAYMET model are daily totals. Equations to parse these totals into sub-daily or hourly values are complex and input intensive, and

consequently, require inputs of meteorological parameters that are also unavailable (e.g., Linacre, 1992; Collares-Pereira and Rabl, 1979).

SolarCalc is a computer model that simulates hourly point values for incident solar radiation. It was recently developed primarily for use in agricultural applications where soil moisture variability is known to directly affect seed germination success, and where incident radiation is understood to be the primary variable controlling the soil moisture conditions (Spokas and Forcella, 2006). Field validation of SolarCalc resulted in predictions that compared well with other empirical solar radiation models; however, SolarCalc has the significant advantage of predicting hourly incoming shortwave radiation for an entire year based on limited climatic data. The only input parameters needed are latitude, longitude, elevation, daily precipitation totals, and daily maximum and minimum temperatures. SolarCalc was used to generate simulated, hourly incoming shortwave radiation values for both the model calibration and the post-fire simulations.

4.2.2 ***Validation Weather Generation.*** The main difference between the methods used to format the weather inputs for the calibration and validation periods involved the data collection frequency of the available meteorological records. Hourly meteorological data from MSO were available for the time period coinciding with the post-fire simulations. These data were entered into a database, which was then queried to select only those measurements taken at 3-hour intervals. Wind speed measurements were available for this period, and these values were used in place of the daily average values used in the calibration run. Incoming longwave and shortwave radiation data were not available, and the procedures used to generate these parameters for the post-fire simulations were identical to those used for the calibration process. Lastly, hourly

precipitation totals were summed over each individual 3-hr interval to produce 3-hr precipitation totals.

4.3 ***CONFIGURATION FILE***. The DHSVM configuration file is an ASCII text file that acts as a look-up table for the physical values describing the spatial inputs into the model. The configuration file tells the model how to interpret the thematic spatial inputs, and hence, is generally where edits are made to affect model outputs. Fine-tuning the physical values describing the spatial inputs into DHSVM takes place in the configuration file.

DHSVM allows for any number of soil or vegetation types in a watershed. In addition, each vegetation type may consist of two separate vegetative layers, and each soil type may consist of any number of soil layers. The list of physical values describing each individual soil and vegetation layer is long. Furthermore, many of the parameters used in model calculations are obscure and are not readily available in the literature for each unique soil and vegetation type. Thorough completion of the configuration file using cited values for soil and vegetation parameters was time-intensive. Some generalization was necessary; however, the goal in this case was to parameterize the model for the calibration run using the best available referenced values. Descriptions of the most relevant input parameters and the sources for these values are given in Tables A1, A2, and A4 in the Appendix.

4.4 ***DHSVM CALIBRATION.*** The process of distributed model calibration involves the optimization of parameter values to provide the best possible fit between measured and simulated hydrologic response (Grayson and Blöschl, 2000). A description of the specific steps taken to calibrate DHSVM to the Eightmile Creek watershed follows.

4.4.1 ***Calibration Methodology.*** Calibration of DHSVM in this application involved both qualitative and quantitative assessments of the goodness-of-fit of simulated streamflow to observed streamflow for over one hundred different parameter configurations. A USGS stream gage was historically located approximately 7.2-km upstream from the confluence of Eightmile Creek and the Bitterroot River. This station continuously recorded daily discharge in ft^3/s for the 1958 – 1963 water years. These gage data were obtained through the National Water Information System web interface (United States Geological Survey, 2005). The water year is the standard measure for the annual hydrologic cycle, and it is named based on the calendar year in which it ends. In the United States, the water year begins October 1 and ends September 30. Any streamflow recorded on October 1 is likely to be representative of the baseflow of a particular stream and is less likely to be influenced by any snowmelt or rainfall within a watershed. The model was run with a starting date of October 1, 1956. Simulated results from the first year were discarded to account for the necessary model spin-up period. 3-hr simulated streamflow values were averaged to identify the daily mean. These values were then graphed against the daily observed values, and the input parameters were adjusted to achieve the best possible fit of the simulated data. Visual assessment of the graphed results identified the best simulations, and statistical analysis of these selected results quantitatively identified the most accurate simulation obtained.

Because DHSVM is physically-based, a thorough understanding of the physics driving the water and energy balance calculations, as well as an understanding of how DHSVM routes these values through a watershed, are key components of successful model calibration. Systematic trial and error proved to be the most effective calibration

method. A 7-yr simulation using DHSVM took approximately five hours of computing time. Simulations were run on a Linux cluster comprised of sixteen 3.2-GHz Xeon processors. Multiple runs were completed simultaneously; however, this slowed down the processing speed considerably. The general strategy involved groups of overnight model runs dedicated to the investigation of the sensitivity of a single input parameter with respect to streamflow at the gage location. All other inputs were held constant while the input value of interest was adjusted to address the range of referenced values. Any improvement or decline in the simulation results was noted. Investigation of the next possible input was dictated both by suggestions made in the literature of the most sensitive model parameters, and observation of the general shape of the simulated hydrograph with respect to the measured values. This process was repeated until the model simulation could be improved no further based on the available input data.

4.4.2 ***Statistical Analysis.*** As suggested by Coffey et al. (2004), three statistical measures were employed to assess the normality of the measured and modeled data prior to statistical analysis of the goodness-of-fit. The statistics used include the Kurtosis value, the skewness coefficient, and the Shapiro-Wilk *W*-Test. Kurtosis values of three indicate a normal distribution. Lower values suggest a more heavily peaked distribution, and higher values represent a more heavily tailed distribution. The skewness coefficient provides a measure of symmetry. Perfectly symmetrical distributions have a skewness coefficient of zero, with higher values indicating more heavily skewed data. The Shapiro Wilk *W*-test calculates the *W* statistic using the sample variance, size, and mean. Normality is assessed using the *W* statistic at a specified level of significance. These tests

of normality were completed using SPSS 13.0. A summary of all of the statistical measures used in this research is provided in Table A5 in the Appendix.

In each case, four model performance statistics were calculated next to assess the goodness-of-fit of the model simulations. The first three statistics are median objective functions and include the normalized median absolute error (*MdAE*), the robust coefficient of determination (*CD**), and the robust modeling efficiency value (*EF**; Zacharias, *et al.*, 1996).

$$MdAE = median\left\{\left|Y_i - X_i\right| : i = 1,2,\mathrm{K}\ ,n\right\} \times \left(\frac{100}{\overline{Y*}}\right) \tag{6}$$

$$CD* = \frac{median\left\{\left|Y_i - \overline{Y*}\right| : i = 1,2,\mathrm{K}\ ,n\right\}}{median\left\{\left|X_i - \overline{Y*}\right| : i = 1,2,\mathrm{K}\ ,n\right\}} \tag{7}$$

$$EF* = \frac{\left\{\left|Y_i - \overline{Y*}\right| : i = 1,2,\mathrm{K}\ ,n\right\} - median\left\{\left|Y_i - X_i\right| : i = 1,2,\mathrm{K}\ ,n\right\}}{median\left\{\left|Y_i - \overline{Y*}\right| : i = 1,2,...,n\right\}} \tag{8}$$

$$\overline{Y*} = median\left\{Y_i : i = 1,2,\mathrm{K}\ ,n\right\} \tag{9}$$

In these equations, Y_i is the observed value, and X_i is the predicted value. Normalized *MdAE* values are expressed in percent. For perfect model fit, *MdAE* = 0, and *CD** = *EF** = 1. The Nash-Sutcliffe efficiency coefficient, *E*, (Nash and Sutcliffe, 1970) was also calculated. *E* is the ratio of the mean absolute error to the variance in the measured data:

$$E = 1 - \frac{\sum_{i=1}^{n}\left(Y_i - X_i\right)^2}{\sum_{i=1}^{n}\left(Y_i - \overline{Y}\right)^2} \tag{10}$$

where $\overline{Y}$ is the average of the observed values. *E* values may range from 1.0 to -∞, and higher values indicate a better fit of the simulated data. An *E* value equal to zero

indicates that the mean of the observed streamflow is as good of a predictor of flow as the modeled results (Legates and McCabe, 1999). A value below zero suggests that the mean value of the observed flows would have been a better indicator of flow (Krause *et al.*, 2005). This regression value is calculated in place of the regression coefficient of determination (R^2), because E is sensitive to the differences in the observed and predicted means and variances and R^2 is not. Because R^2 is insensitive to these parameters, large R^2 values can be obtained even for very poor model simulations (Legates and McCabe, 1999).

For the post-fire simulations, three additional goodness-of-fit statistics were calculated for the 2006 water year because the median objective functions described above failed to assess accurately the model performance. These statistics are essentially the mean-based origins of the median objective functions used. They include the normalized root mean square error (*RMSE*), the coefficient of determination (*CD*), and modeling efficiency value (*EF*; Loague *et al.*, 1988):

$$RMSE = \left[\left(\frac{1}{n}\right)\sum_{i=1}^{n}\left(Y_i - X_i\right)^2\right]^{0.5}\left(\frac{100}{\overline{Y}}\right) \quad \textbf{(11)}$$

$$CD = \frac{\sum_{i=1}^{n}\left(Y_i - \overline{Y}\right)^2}{\sum_{i=1}^{n}\left(X_i - \overline{Y}\right)^2} \quad \textbf{(12)}$$

$$EF = \frac{\sum_{i=1}^{n}\left(Y_i - \overline{Y}\right)^2 - \sum_{i=1}^{n}\left(Y_i - X_i\right)^2}{\sum_{i=1}^{n}\left(X_i - \overline{Y}\right)^2} \quad \textbf{(13)}$$

4.5 ***DHSVM VALIDATION.*** Model validation describes the testing of modeled simulations using a calibrated model against real data that were not a part of the calibration process (Grayson and Blöschl, 2000). This research aimed to validate DHSVM as an effective cumulative effects assessment tool for use in forested, snow-dominated, fire-affected watersheds of western Montana. This goal was met through the comparison of measured to modeled streamflow using the calibrated DHSVM following a near catchment-wide forest fire in the Eightmile Creek watershed.

Spatial inputs of landscape characteristics into DHSVM version 2.0.1 are static. The vegetative cover, soil type, and road and stream network parameters do not change over the course of a simulation. Because DHSVM is highly adaptable, the model design allows the user to manipulate landscape characteristics and run the model for different landscape scenarios. This theoretically allows the user to quantitatively assess the effects of cumulative management actions or natural disturbances on the hydrology of a watershed. Specifically, a DHSVM user should be able to manipulate the landscape to reflect the soil and vegetation properties following a forest fire. The results of the different simulations are analyzed to assess the effects that a particular landscape change may have on the hydrologic regime of a drainage basin.

4.5.1 ***Simulated fire disturbance with DHSVM version 2.0.1***. A vegetation burn severity grid of the Cooney Ridge Fire Complex was used to reclassify the vegetation inputs in the Eightmile Creek watershed following the fire. This grid was then used in DHSVM version 2.0.1 in order to simulate the fire-affected watershed landscape. Changes to the vegetation following the fire were made according to a general set of logic. This set of logic was developed with consideration paid to referenced burn

severity data, the dominant hydrologic processes affecting runoff in a snowmelt-dominated system, and general knowledge of the burn characteristics of the Eightmile Creek watershed based on personal observations. The soil burn severity classification for the entirety of the Cooney Ridge Fire was classified as low (Lolo Burned Area Emergency Recovery Team, 2003). According to this burn severity classification, no spatially or temporally significant changes should be expected with respect to the hydrologic properties of the fire-affected soils. Thus, no changes were made to the soil inputs in the DHSVM version 2.0.1 post-fire simulation.

Using the Reclassify Tool in ArcMap 9.1, the vegetation grid was reclassified to represent the burned landscape. Several different groups of logical criteria were used to reclassify the vegetation grid, and these different grids were subsequently used in the DHSVM simulations. However, because the burn severity data was so coarse, differences in the alternate burned vegetation grids were minor. Thus, the simulations utilizing these different vegetation grids produced nearly identical results. The vegetation grid that was ultimately utilized to represent the burned landscape in DHSVM was generated from the following logical assertions:

- All unburned cells retained their original pre-burn vegetation designation.
- All cells affected by high severity fire behavior, regardless of vegetation type, were converted to burned, bare ground.
- Cells affected by low or medium severity burns and classified as grassland or bare ground were reclassified as burned, bare ground. Burned, bare ground was not hydrologically different from unburned bare ground.

- Cells affected by low or medium severity burns and classified as shrublands were converted to burned shrublands characterized by a 50% reduction in the monthly LAI values.
- Cells affected by low severity burns and classified as vegetation types with a forest canopy were edited to reflect total removal of the understory and an undisturbed overstory.
- Cells affected by medium severity burns and classified as forested vegetation types were edited to reflect total removal of the understory and a 50% reduction in the overstory tree density and monthly LAI values.

DHSVM version 2.0.1 was run using a 3-hr time step and the altered vegetation grid for the 2003 to 2006 water years. As in the calibration process, the first year of simulated data (2003) was discarded to account for the necessary model spin-up period. The results of these streamflow simulations were compared to measured streamflow data collected for the 2004 to 2006 snowmelt seasons. These data were obtained by Michael Roberts from the Montana State Department of Natural Resources and Conservation (DNRC; 2006). Roberts installed an Aquarod on the mainstem of Eightmile Creek, 6-km upstream of the original USGS gage location, in the spring of 2004, and a year after the Cooney Ridge Fire. The device logged daily stream stage data during the snowmelt season. Using a rating curve constructed by Roberts the stage information was then converted to daily flow values (in ft^3/s), which were used to assess the performance of the post-fire model simulations (2006).

4.5.2. Simulated fire disturbance with the DHSVM fire model. The DHSVM fire model was used to simulate runoff for the same watershed and time period in order to

compare the performances of each model version with respect to modeling the hydrology of burned landscapes. As in the DHSVM version 2.0.1 validation, the fire model was run at the 3-hr time step for the 2003 to 2006 water years, discarding the first year of simulations just as in the previous scenarios. All input parameters remained constant between the two model versions, with the exception of the input vegetation grid. These results were compared to the model performance of DHSVM version 2.0.1 in a post-fire scenario to assess which model version provided the most accurate simulation.

5. RESULTS

5.1 ***DHSVM CALIBRATION*****.** DHSVM performed well with respect to the calibration of the model to the Eightmile Creek watershed. The results of the simulation with the best fit to the measured streamflow data are shown in Figure 15. Visual assessment of these results suggests that the model performed considerably better some years and considerably worse others. The 1961 water year is shown separately to highlight it as the most accurately simulated year. Statistical analysis of the goodness-of-fit of these data will help to quantify the performance of DHSVM.

Figure 15 – *Calibration results for the Eightmile Creek watershed*. Simulated daily average streamflow (ft^3/s) using DHSVM version 2.0.1 versus measured streamflow at the historic USGS stream gage for the 1958 – 1963 water years (top panel). Bottom panel illustrates the accurate simulations produced for the 1961 water year.

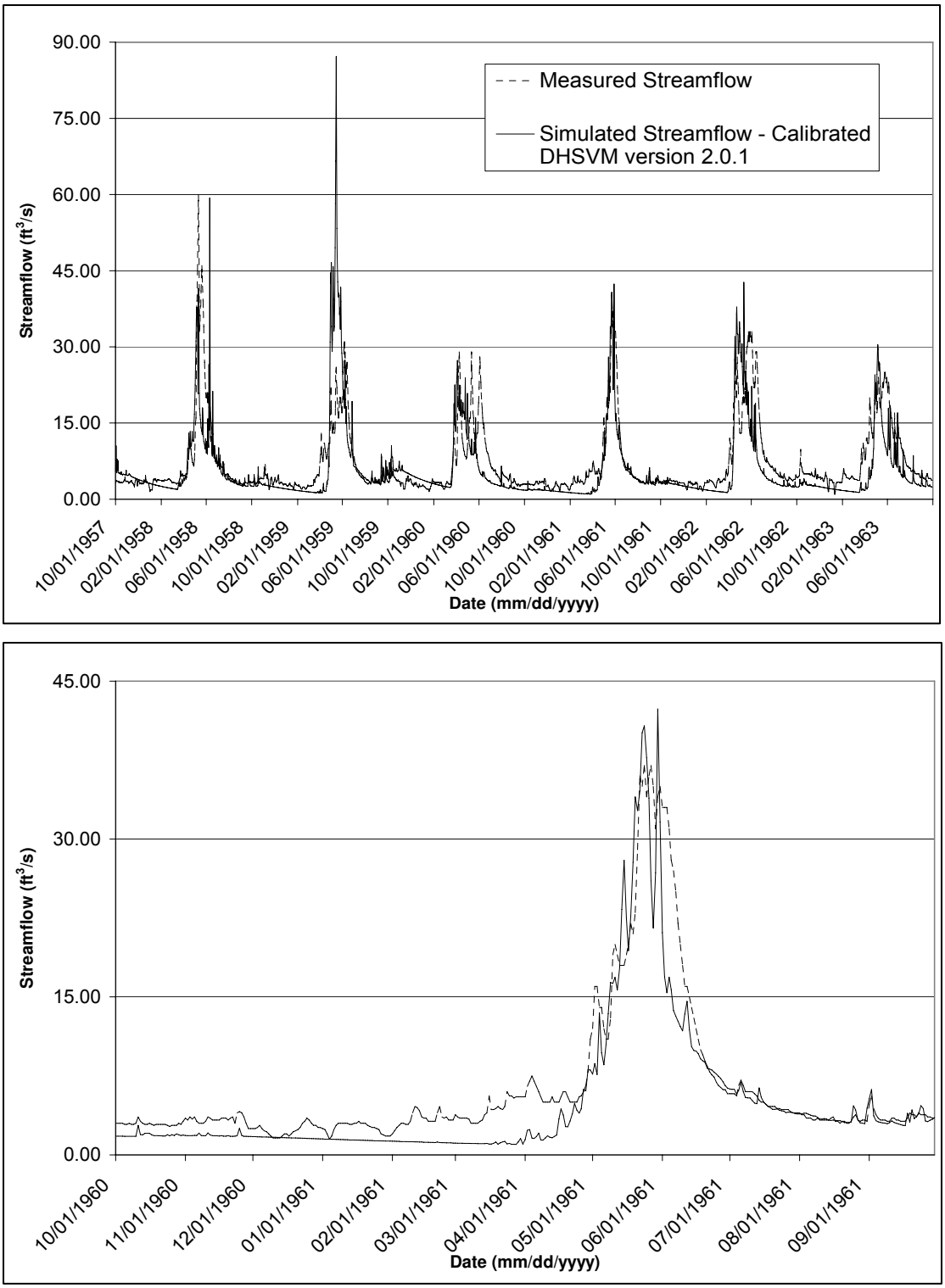

5.1.1 ***Statistical analysis*****.** For both the observed and simulated datasets, all three calculated measures of normality indicate non-normal distribution (Table 2). Therefore, the assumption of normality cannot be presumed for any of the calibration datasets for the purposes of statistical analysis. Because these data do not follow a normal distribution, mean based functions are not necessarily appropriate for an assessment of goodness-of-fit. The median objective functions previously described are more appropriate for non-normally distributed data than are their mean-based origins. Descriptive statistics and measures of goodness-of-fit appropriate for non-normally distributed data were calculated for the entire simulation period, as well as for individual water years. These results are displayed in Tables 3 and 4, respectively.

Table 2 – ***Normality testing results for measured and simulated calibration data*****. For each dataset, Kurtosis values greater than 3 indicate a heavily right-tailed distribution, and positive Skewness coefficients above 1 indicate asymmetrically distributed data skewed to the right. The Shapiro-Wilk Test, performed at the confidence level of α = 0.5, and using the null hypothesis that the data within each set were normally distributed, also finds that neither dataset is normally distributed.**

	Kurtosis	Skewness	Shapiro-Wilk Test	
Data	**Value**	**Coefficient**	**P-value**	**Conclusion**
1958 - 1963 daily flows			h_0: the data are normally distributed	
Observed	7.45	2.55	0.000	Reject h_0
DHSVM simulated	14.68	3.45	0.000	Reject h_0

Descriptive statistics calculated include the sample mean, median, minimum value, maximum value, and standard deviation for each of the observed and simulated datasets for the entire continuous 6-yr period of record, as well as for each individual water year. Table 3 presents these statistics for the entire period of record, and summarizes the individual water year statistics by presenting the difference between the simulated and

observed statistic. These measures of range and central tendency for the independent datasets provide an idea of how well the distribution of the simulated data matches the distribution of the measured data. When compared to the measured data, DHSVM version 2.0.1 simulations generally had a lower mean, median and standard deviation, and a higher maximum value. The minimum values tended to be approximately equal. These statistics illustrate that the DHSVM simulated yearly snowmelt was characterized by a more narrow distribution with slightly higher peaks, a shorter time-to-rise, and more steeply sloping rising and recession limbs when compared to the distribution of the measured flows. These patterns are readily apparent in the bottom panel of Figure 15, depicting the modeled versus measured streamflow for the 1961 water year.

Table 3 – ***Descriptive statistics for the DHSVM calibration to the Eightmile Creek watershed*****. Observed and DHSVM simulated average daily streamflow (ft^3/s) datasets for the 1958 – 1963 water years are described. Single statistics are presented for the observed and simulated datasets for the entire period of record, while the deviation of the simulated statistics from the observed statistics are presented for each individual water year.**

	Period of Record 1958 - 1963			Individual Water Years (Simulated - Observed)					
	Obs*	**Sim****	**Dif*****	**1958**	**1959**	**1960**	**1961**	**1962**	**1963**
Mean	7.2	5.1	-2.1	-1.2	1.1	-0.8	-1.4	-2.0	-3.1
Median	4.0	3.1	-0.9	0.2	-0.9	0.1	-1.6	-1.1	-2.3
Min. Value	1.0	1.0	0.0	0.4	-0.7	0.3	-0.5	-0.3	0.3
Max Value	60.0	87.2	27.2	-0.7	56.2	-1.7	5.4	9.7	5.4
St. dev.	7.3	3.1	-4.2	-3.0	6.3	-0.9	-0.3	-0.1	-0.5

* Obs = observed

** Sim = simulated

*** Dif = Difference (Simulated - Observed)

Model performance statistics calculated include the *MdAE*, *CD**, *EF**, and *E* statistics. *MdAE* values less than 50%, and *EF** and *CD** values ±0.5 from the target

value of 1.0, indicate satisfactory results concerning goodness-of-fit of hydrologic simulations to measured streamflows (Coffey *et al.*, 2004). *E* values greater than 0 indicate that when compared to the mean value of the measured data, the modeled values are better predictors of streamflow amounts. Negative *E* values suggest the opposite. The goodness-of-fit statistics calculated for the calibration data suggest good model performance. The *MdAE* values were below the 50% target threshold for all six of the water years simulated (Table 4). The *CD** statistics were at or above the 0.5 deviation from a perfect fit of 1.0 for four of the six water years. The *EF** statistic provided a less promising picture of DHSVM performance, as it did not fall within the target area for any of the six simulated years. The *E* statistic also indicates less consistent simulation success; however, the average value for the entire period of record is colored by one poorly simulated year (1959; Table 4).

Table 4 – *Goodness-of-fit statistics for the DHSVM calibration to the Eightmile Creek watershed. MdAE*, *CD, *EF**, and *E* statistics were calculated to assess the performance of DHSVM version 2.0.1 for the 1958 – 1963 water years.**

	Period of Record	Individual Water Years					
	1958 - 1963	1958	1959	1960	1961	1962	1963
MdAE	37.91	30.21	26.90	43.55	33.66	44.22	47.09
CD*	0.57	0.49	0.53	0.86	0.42	0.57	0.50
EF*	-0.52	-1.03	-0.02	-0.38	-0.47	-0.92	-0.81
E	0.33	0.53	-1.06	0.25	0.81	0.44	0.36

MdAE = Normalized median absolute error (in percent); for perfect fit, MdAE = 0
CD* = Robust coefficient of determination; for perfect fit CD* = EF* = 1
EF* = Robust modeling efficiency value
E = Nash-Sutcliffe regression coefficient; for perfect fit E = 1

5.2 DHSVM VALIDATION AND MODEL VERSION COMPARISON. The calibrated DHSVM version 2.0.1 and the DHSVM fire model were both used to simulate runoff in the post-fire landscape of the Eightmile Creek watershed. Because each model

version accounts for fire effects on hydrology in a different way, the calibrated inputs in order to compare the performance of each model version in a post-fire setting. The results of these simulations are displayed in Figures 16 and 17.

Overall, the results of the validation and model comparison efforts were inconclusive. Compared to DHSVM version 2.0.1 (Figure 16), the DHSVM fire model more accurately captured the post-fire snowmelt dynamics in the Eightmile Creek watershed (Figure 17). However, subsequent statistical analysis suggests that these improvements are slight.

Figure 16 – *Simulation results for the Eightmile Creek watershed using DHSVM version 2.0.1 in a post-fire landscape*. Measured daily snowmelt runoff (ft^3/s) logged at the Sluice Creek confluence is graphed against daily simulated flow (ft^3/s).

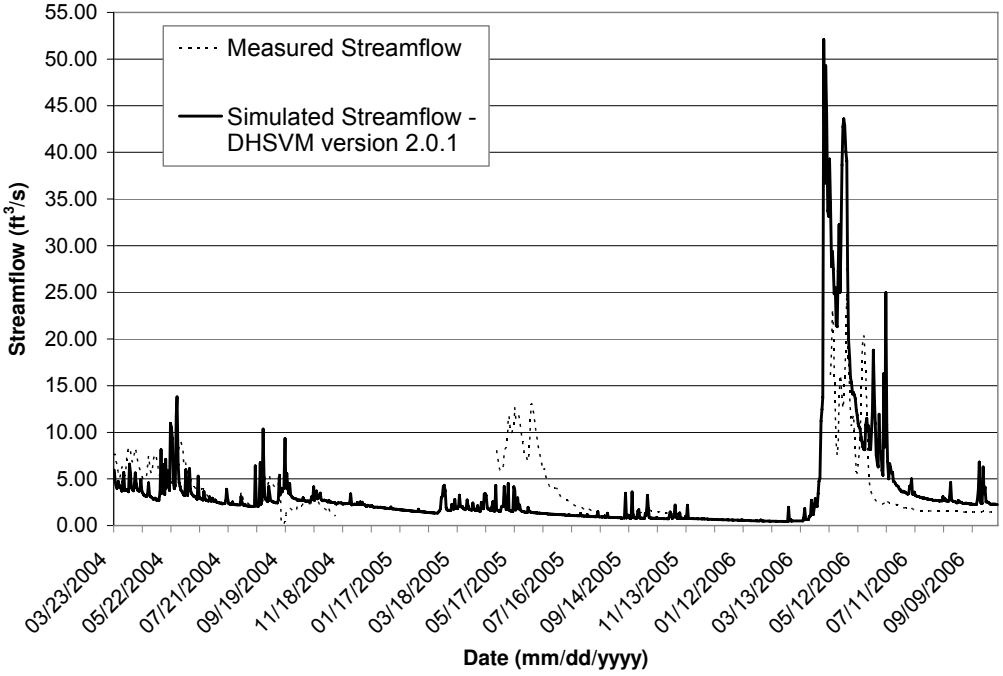

Figure 17 – *Simulation results for the Eightmile Creek watershed using the DHSVM fire model in a post-fire landscape*. Measured daily snowmelt runoff (ft^3/s) logged at the Sluice Creek confluence is graphed against daily simulated flow (ft^3/s).

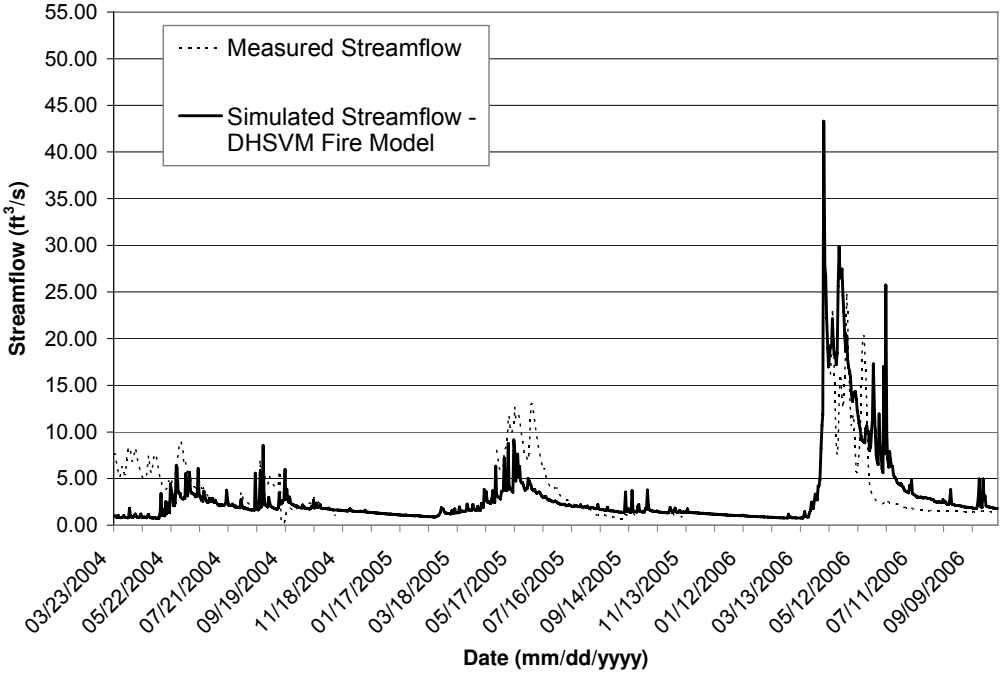

5.2.1 ***Statistical analysis*****.** Descriptive statistics and statistical measures of goodness-of-fit were calculated in the same fashion as they were for the calibration datasets, with the supplementation of the mean-based functions calculated for the 2006 snowmelt season. In addition, because the post-fire measured streamflow data are not continuous, it is inappropriate to report statistics for the entire period of record. The results of these analyses are displayed in Tables 5 and 6 respectively.

Table 5 – ***Descriptive statistics for the post-fire DHSVM simulations in the Eightmile Creek watershed*****. Statistics describing the observed and simulated average daily streamflow (ft^3/s) were calculated. Differences between the statistics describing the observed data and the statistics describing the simulated data (using both DHSVM version 2.0.1 and the DHSVM fire model) are presented.**

	Individual Snowmelt Seasons (Simulated - Observed)					
	2004		**2005**		**2006**	
	DHSVM	**FM**	**DHSVM**	**FM**	**DHSVM**	**FM**
Mean	-0.5	-1.9	-2.4	-1.2	3.6	2.3
Median	-0.9	-1.9	-0.7	0.2	1.8	1.8
Min. Value	1.9	0.6	0.2	0.8	0.8	0.4
Max. Value	4.8	-0.5	-8.6	-4.0	18.7	5.0
St. dev.	-0.4	-1.0	-2.9	-2.1	3.8	1.0

*Obs = observed

**DHSVM = DHSVM version 2.0.1; (Simulated - Observed)

***FM = DHSVM fire model; (Simulated - Observed)

There are few obvious patterns in the descriptive statistics of the post-fire simulations for both model versions. The 2004 and 2005 water year simulations had similar distribution characteristics. For each of these two years, and with each model version, when compared to observed streamflow, simulation distributions tended to have higher minimum values and lower means, medians, maximum values, and standard deviations (Table 5). 2006 was unique in that the modeled simulations using each model version produced higher values for each descriptive statistic calculated, when compared to

observed values. With respect to model version comparison, the DHSVM fire model distribution more closely matched the observed streamflow distribution for two of the three water year simulations (2005 and 2006; Table 5), as evidenced by the smaller observed differences in the calculated descriptive statistics.

The goodness-of-fit statistics calculated for the post-fire simulations using DHSVM version 2.0.1 and the DHSVM fire model provide a mixed picture of model performance (Table 6). Visual assessment of the simulated hydrographs displayed against measured streamflow (Figures 16 and 17) suggests that when compared to the calibration results, neither model version performed as well in the post-fire application. However, the goodness-of-fit statistics do not entirely support this assertion. For example, the 2004 water year had relatively low *MdAE* values for each model version, indicating good model fit. In addition, *CD** values were within 0.5 of unity (Table 6), which is the target fit threshold previously described. In addition, the *EF** values, while not within the target threshold of ±0.5 of 1.0, were closer to 1.0 than for any of the calibration years, suggesting that the post-fire simulations fit the measured data more accurately. In contrast, *E* values were negative for each model version in 2004 (Table 6), indicating essentially no fit.

Table 6 – ***Goodness-of-fit statistics for the post-fire DHSVM simulations using DHSVM version 2.0.1 and the DHSVM fire model.***

	Individual Snowmelt Seasons					
	2004		2005		2006	
DHSVM Version	v 2.0.1	Fire Model	v 2.0.1	Fire Model	v 2.0.1	Fire Model
MdAE	29.32	25.89	45.68	36.01	94.68	89.59
CD*	1.41	0.81	1.06	2.20	0.13	0.14
EF*	0.28	0.36	-0.03	0.19	-5.56	-5.21
E	-0.10	-1.18	-0.30	0.41	-0.54	0.26
RMSE					43.11	29.84
CD					0.31	0.64
EF					-0.17	0.17

MdAE = Normalized median absolute error (in percent); for perfect fit, MdAE = 0
CD* = Robust coefficient of determination; for perfect fit CD* = EF* = 1
EF* = Robust modeling efficiency value
E = Nash-Sutcliffe regression coefficient; for perfect fit E = 1
RMSE = Normalized root mean square error (RMSE); for perfect fit, RMSE = 0
CD = Coefficient of determination; for perfect fit CD = EF = 1
EF = Modeling efficiency value

When compared to the visual assessment of the graphs of measured versus simulated streamflow for the 2006 water year (Figures 16 and 17), the values for the median-based statistics paint a contradictory picture of model performance. The graphed results suggest somewhat satisfactory model performance, particularly for the DHSVM fire model version; however, the median-based statistics suggest lack of satisfactory fit for each of the four statistics calculated. Because the median-based functions failed to accurately assess model performance for the 2006 water year, the mean-based origins of these statistics were calculated in order to provide some clarification. The values for the mean-based statistics better correspond with the visual assessment of the graphs of measured versus simulated streamflow (Figures 16 and 17). The DHSVM fire model slightly outperformed DHSVM version 2.0.1 in the post-fire landscape for the 2006 water year.

6. DISCUSSION

6.1 *CALIBRATION RESULTS*. Overall, DHSVM was relatively well calibrated to the Eightmile Creek watershed. The model was able to accurately simulate the general shape of the measured hydrograph for each of the six modeled water years. Based on the 6-yrs of continuous daily streamflow data, DHSVM tended to slightly underestimate baseflow and somewhat overestimate peakflow.

Of particular interest in hydrologic modeling applications is the ability of a model to simulate the shape of the hydrograph recession limb. Because this portion of the hydrograph is dominated by snowmelt processes, the slope of the recession limb curve is more of a reflection of the physical characteristics of a particular watershed than it is a reflection of precipitation inputs. Therefore, if the recession limb slopes of the simulated streamflow match the recession limb slopes for the measured streamflow, then the input values used to physically characterize the watershed being modeled can be considered accurate. Thus, the model is calibrated to that particular watershed. In this research, DHSVM generally simulated the correct slope of the hydrograph recession limb for each of the six simulated water years; however, the model predicted a slightly earlier recession onset than was measured for three of the six water years. The success of the calibration efforts is particularly surprising when one considers the significant limitations presented by the lack of any sub-daily or high-elevation meteorological data corresponding with the 1958 – 1963 water years.

Based on visual assessment of the simulated hydrographs, DHSVM produced a particularly good fit to measured streamflow for the 1961 water year (Figure 15, bottom panel). This is statistically quantified by the high value for the calculated Nash-Sutcliffe regression coefficient ($E = 0.81$), as well as a relatively low value for the normalized

median absolute error (*MdAE* = 33.66; Table 4). In contrast, Figure 15 suggests that the 1959 water year streamflow was poorly simulated by DHSVM. However, the goodness-of-fit statistics calculated for the individual water years do not fully support this initial observation. The Nash-Sutcliffe regression coefficient suggests essentially no fit between the measured and simulated data for 1959 (*E* = -1.06) and appears to be in accord with the visual assessment. In contrast, the normalized median absolute error is actually lower (*MdAE* = 26.90), and therefore suggests a better simulation than that produced in 1961. This discrepancy may be explained by the descriptive statistics (Table 3). Although the modeled flow appears to fit poorly to the measured flow for 1959, the median yearly flow values for the simulated and measured data are similar (2.9 and 3.8, respectively). For the 1961 water year, the simulated and measured medians are not as comparable (1.9 and 3.5, respectively). Because the *MdAE* statistic is calculated using the median, this may explain why this statistic indicates a better fit for the poorly simulated 1959 data.

Another possible explanation is given by the Nash-Sutcliffe regression coefficient (*E*). Because *E* is calculated based on the squared differences in observed and simulated values, the statistic tends to overestimate peak flows and neglect low flows. This directly translates to overestimation and underestimation of model performance during these different periods of flow (Krause *et al.*, 2005). For the 1959 simulation, DHSVM significantly overestimates the magnitude of the peak. The Nash-Sutcliffe efficiency coefficient for the 1959 measured and modeled data would be disproportionately affected by this fact. Closer visual examination of the 1959 simulated hydrograph (Figure 15) reveals that DHSVM accurately models the recession limb and simulates baseflow no

better or worse than for any other year. The *E* statistic would be colored by the overestimation of the modeled peak, while the *MdAE* value would not necessarily be as affected by this peak.

A purely physical model should not technically need calibration. Nevertheless, because the algorithms in DHSVM are approximations, because drainage basin parameters are estimates, and because meteorological forcings are uncertain, DHSVM should be calibrated to measured values before it is validated (Doten *et al.*, 2004). Logical adjustments of input parameters throughout the course of fine-tuning the model simulations were successful in bringing the simulated results more closely in line with measured values. The input adjustments that appeared to have the greatest impact on the simulation results included changes made to the value used to represent saturated soil hydraulic conductivity, the wind speed reference height, and the meteorological data used to drive the model.

DHSVM was particularly sensitive to the soil input parameters affecting lateral soil saturated hydraulic conductivity (*K*). The model developers assert that *K* is the single greatest calibration parameter (DHSVM Administrator, 2006B). Figure 18 displays 1-yr of the results of four independent model simulations run for 6-yrs during the calibration period. The only difference between each simulation is a change in the order of magnitude for the lateral *K* value of the gravelly silt loam soils. These values were edited in order isolate the effects that changes in the *K* values had on model performance. The results are graphed against the measured streamflow data.

Lateral *K* values on the order of E-05 (*K* = 1.88E-05) produced the most accurate simulations in the case of the Eightmile Creek watershed calibration. These values were

ultimately incorporated into the calibrated model applied in the post-fire setting. Figure 18 suggests that decreasing the order of magnitude for the lateral *K* values reduced the overall flashy nature of the hydrograph, but only to a point, beyond which the simulations degraded. The highest value used (*K* = 1.88E-03) caused the model to predict excessively high peakflows and unnaturally steep rising and recession limbs. Increasing the lateral *K* values for the soil profiles can be likened to opening the pipes, enabling water from rain or melting snow to move quickly through the soil profile and out of the watershed. Decreasing the lateral *K* values progressively produced lower peaks and more closely matched the timing and slopes of the measured hydrograph. However, for values below the order of magnitude of E-05, the simulations began to degrade. This may be explained by the fact that as the *K* values and associated maximum infiltration rates decrease and approach zero, water on a steep landscape is more prone to run over the soil surface rather than infiltrate into the soil profile. Water moving over the landscape will tend to move across and exit the watershed more quickly than if it was contained in the soil profile. This produces a simulated snowmelt hydrograph that is equally as flashy as a simulated hydrograph produced with excessively high *K* values.

Figure 18 – *Saturated hydraulic conductivity input effects*. Measured streamflow at the Eightmile Creek USGS stream gage versus DHSVM simulated flow. The only difference between simulations involves the orders of magnitude for the lateral saturated hydraulic conductivity value for the gravelly loam soil type input into the model. *K* = 1.88E-05 produced the most accurate simulations. Increasing or decreasing the value of *K* away from this E-05 threshold resulted in progressively less accurate simulations.

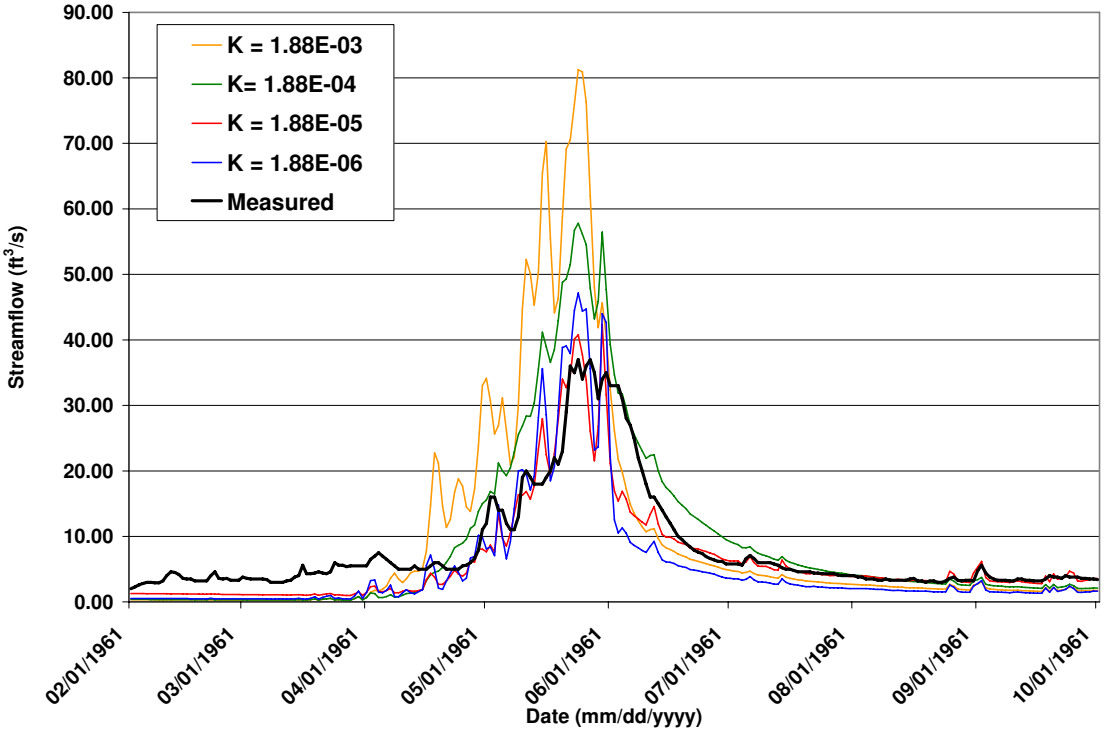

The model also appeared to be particularly sensitive to an input factor called the reference height. This numeric value represents the height above the ground, in meters, where the wind speed measurements used in the meteorological drivers in the model were taken. The value for this factor becomes particularly important in a snow-dominated system where the aerodynamic forces affecting wind movement above and through a forest canopy tend to control snow accumulation and ablation patterns, and therefore ultimately control the shape of the hydrograph.

Figures 19 and 20 illustrate the effect of changing the reference height while holding all other inputs constant. The suggested value for use in the reference height input is a value equal to approximately 10-m above the height of the tallest canopy present in the watershed being modeled (DHSVM Administrator, 2006B). The tallest canopy in both the pre- and post-fire simulations for the Eightmile Creek watershed was estimated at 30-m. In this model calibration, the use of a reference height value below 30-m resulted in significant model instability (Figure 19), and DHSVM predicted unrealistic peakflows. Annual peak discharge was recorded at the USGS gage on Eightmile Creek from 1957 until 1972. The average annual peakflow for Eightmile Creek calculated from these 15-yrs of data is 56.5-ft^3/s (United States Geological Survey, 2005). DHSVM simulations using a 25-m reference height and a 30-m tall forest canopy predicted annual peak flows averaging around 500-ft^3/s (Figure 19). Flows of this magnitude are not reasonable for Eightmile Creek.

Figure 19 – *The effects of insufficient reference height values*. Measured streamflow at the Eightmile Creek USGS stream gage versus DHSVM simulated flows with different reference height values input into the model. The 40-m reference height is above the forest canopy, whereas the 25-m reference height is below the forest canopy and illustrates the resulting model instability.

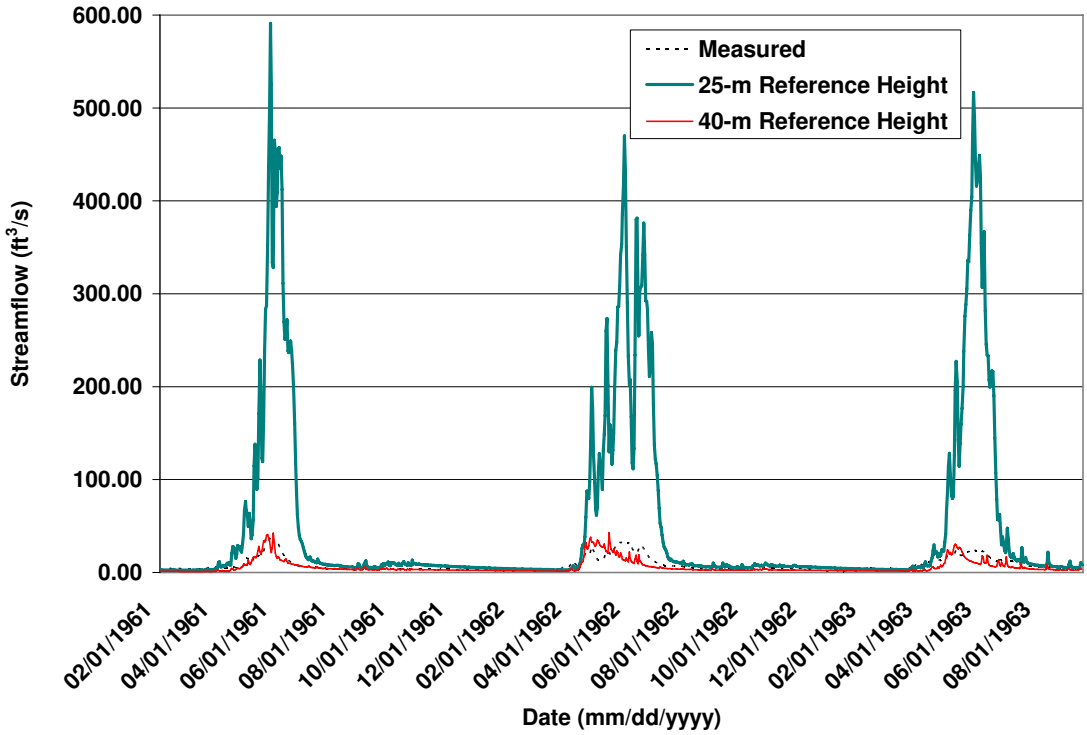

Figure 20 illustrates the effect of increasing the reference height beyond the recommended level of 10-m above the tallest canopy. Although this does not greatly affect the hydrograph, peaks become generally more exaggerated with increasing reference height values, thus degrading model accuracy.

Figure 20 – *The effects of excessive reference height values.* Measured streamflow at the Eightmile Creek USGS stream gage versus DHSVM simulated flow with different reference height values input into the model. Both values are above the 30-m forest canopy, and therefore, changes have little effect on model simulations.

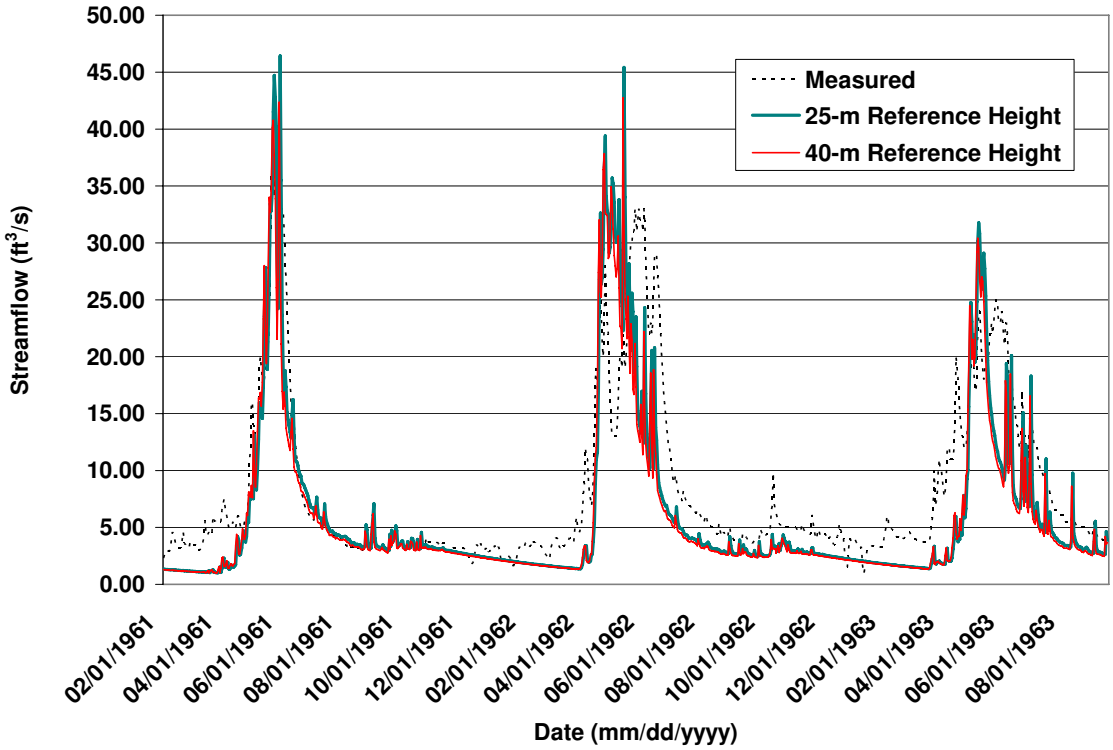

When simulating hydrologic response, the spatial distribution of meteorological parameters over a catchment is potentially the most crucial component of the modeling process (Alila and Beckers, 2001). Perhaps this is why the interpolation process also appeared to significantly affect the modeled streamflow. DHSVM uses one of three different user selected interpolation methods to spatially distribute the meteorological data across a watershed. The methods available are inverse distance weighted, nearest, and variable Cressman. The inverse distance weighted approach uses a weighted mean of the data per time step at each point location for the meteorological records. These weighted means are inversely proportional to the squared distance between the

interpolated value and each data point (Blöschl and Grayson, 2000). The nearest method assigns values in each cell equal to that of the weather station nearest to the cell. The variable Cressman method functions similarly to the inverse distance system, but the user can define a distance equal to the radius of influence from each station (DHSVM Administrator, 2006B).

The interpolation method of choice becomes significant when there is more than one weather station within, or in close proximity to the drainage basin boundary. Because the only weather data available for calibration were recorded at a location 31.6-km northwest of the mouth of Eightmile Creek, virtual weather stations were created within the watershed boundary in order to better address the spatial variability of the meteorological parameters in a steep watershed. Temperature and precipitation data were generated for each virtual station using Missoula data according to constant orographic lapse rates and the difference in elevations. Incoming longwave radiation values were calculated as described in the methods section, using the appropriate lapsed temperature values instead of the recorded Missoula temperatures. Incoming shortwave radiation values were generated with the SolarCalc application. These SolarCalc simulations were driven by the location, elevation, and lapsed temperature and precipitation parameters of the virtual weather station. Relative humidity and wind speed data remained unchanged from the original Missoula values.

Initial model runs utilized the Missoula International Airport (MSO) as the sole weather station. Because MSO is located at the bottom of the Missoula Valley, and a significant distance from the mouth of the Eightmile Creek watershed, utilization of this station alone to drive DHSVM simulations for the Eightmile Creek catchment were

unsuccessful. The model was unable to apply accurate temperature and precipitation lapse rates to produce a realistic snowpack within the watershed. The resulting simulated hydrographs were well below measured values.

In an attempt to better represent the effects of elevation on the weather patterns in the Eightmile Creek watershed, numerous different virtual weather stations located within the watershed boundary were subsequently generated. Eventually, data were generated to support five different virtual stations, distributed evenly across the watershed. The model was run with various combinations, including one or more of the five virtual stations and the Missoula International Airport. Different interpolation methods were employed for each of these weather station combinations. Ultimately, the best simulation was produced using two centrally located mid-elevation virtual stations and the variable Cressman interpolation method. These results suggest that user intervention to manually force temperature and precipitation lapse rates may be necessary for improved DHSVM simulations in areas with sparse meteorological data and orographically controlled weather.

Overall, DHSVM calibration might have been significantly improved by the existence and use of an additional independent weather data source from within the watershed boundary or nearby at a high elevation. Additionally, another possible source of error in calibration may be the drainage density of the delineated stream network. Drainage density in a watershed reflects the effectiveness of surface runoff and erosion. It also influences the concentration time of flow in a channel network. Because the generation of the stream network as a preprocessing step in DHSVM is prohibitively time intensive, there was no investigation of the effects of alternative drainage densities on

simulated streamflow. The source area threshold value of 0.04-km^2 is a high value for a 4th order watershed with a relatively dry climate. Decreased drainage density would theoretically delay the hydrologic response to storms and snowmelt. Because of the increased distance to a channel, water would be forced to move further downhill through the soil profile before it is intercepted by the road or stream network. This may, in turn, reduce the size of the peaks in the simulated flows and result in a better-calibrated model.

6.2 *VALIDATION AND MODEL VERSION COMPARISON RESULTS.* The results of the DHSVM simulations in the post-fire Eightmile Creek watershed were mixed. In general, DHSVM validation was not as successful as model calibration. When compared to the pre-fire simulations, in the post-fire landscape, neither version of the model matched measured flows as consistently. The calculated goodness-of-fit statistics support this assertion. *MdAE* values for the post-fire snowmelt seasons (Table 6) tended to be greater than the *MdAE* value calculated for the entire calibration period (Table 4), indicating decreased accuracy in the simulations. The *E* statistics also demonstrate this same trend, with values closer to one indicating improved fit, suggesting better overall simulations during the calibration period. Three potential explanations for this observation include abnormal weather patterns for two of the three simulated water years following the fire, inconsistencies in streamflow data collection equipment and locations, and the use of a coarse fire severity grid to dictate fire-induced soil and vegetation changes.

The 2004 and 2005 water years were characterized by below-average winter precipitation. The snow water equivalent (SWE) for the Bitterroot River watershed was below average most of the year in 2004 and well below average for the entire year in

2005. In contrast, the 2006 SWE totals were generally above average (Figure 21; Natural Resources Conservation Service, 2006B). The sparse snowpack during the 2004 and 2005 snowmelt seasons resulted in atypical hydrographs for these water years. There was little variation in the streamflow magnitude for either version of DHSVM to capture. In addition, the first significant peakflows came nearly 3-yrs after the Cooney Ridge Fire. By this point, significant vegetative recovery of the understory had taken place, and the hydrologic system had stabilized to some degree. The potential for destructive flows due to changes in the timing and intensity of runoff following forest fire was not realized in the Eightmile Creek watershed following the Cooney Ridge Fire.

Figure 21 – ***Percent deviation from monthly average snow water equivalent values for the Bitterroot River watershed and the 2004-2006 winter months*** **(Natural Resources Conservation Service, 2006).**

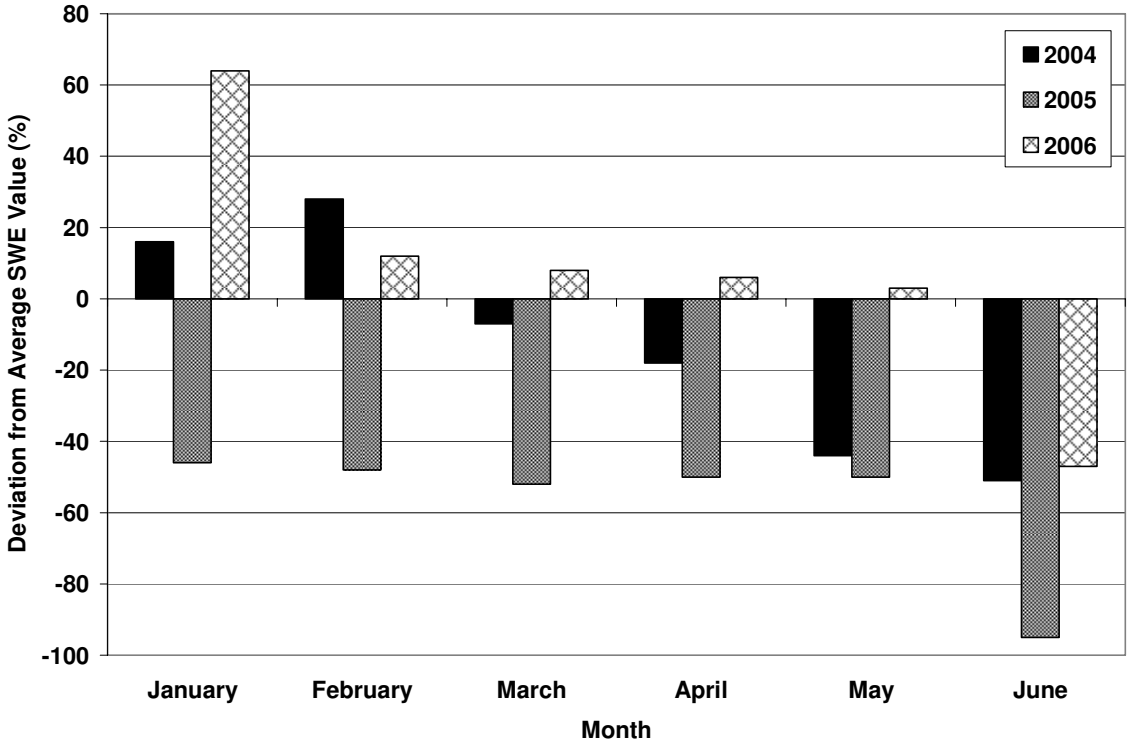

The streamflow data used in the DHSVM calibration were collected by the USGS at a location along the main stem of Eightmile Creek, approximately 7.2-km upstream of the confluence with the Bitterroot River. Daily peak flow was recorded continuously for the 1958 – 1963 water years. In comparison, daily streamflow data were collected after the fire by the DNRC. An AquaRod stage recorder (Figure 22; Roberts, 2006) was seasonally installed in early spring approximately 6-km upstream of the original USGS gage (Figure 23). Stage data were converted to daily flow values using a rating curve. The resulting differences in contributing watershed area and instrumentation at each gage may have led to some inconsistencies between the measured data sets used for goodness-of-fit comparisons in the calibration and model validation exercises.

Figure 22 – ***DNRC AquaRod stream gage on Eightmile Creek at the confluence with Sluice Creek*** **(Roberts, 2006).**

Figure 23 – *Eightmile Creek watershed stream gage locations.*

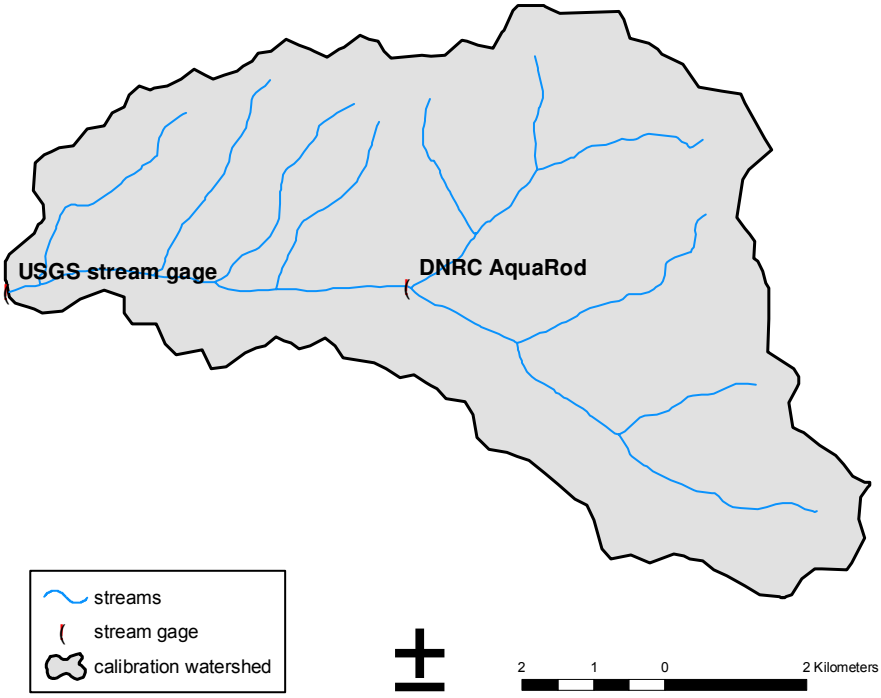

Another contributing factor with respect to model validation results may involve the level of detail of the fire severity grid used to control the post-fire soil and vegetation changes. The spatial data provided by the Lolo BAER Team included a shapefile with rough polygons of vegetation burn severity classification, developed according to observations made in the field immediately following the fire. Vegetation and soil characteristics were altered for use in DHSVM based on the low, medium, or high burn severity classifications presented in this report (Lolo Burned Area Emergency Recovery Team, 2003). While this level of detail may be sufficient for general landscape assessments following fire, it may prove insufficient for modeling post-fire hydrologic response using high-resolution distributed models. A Normalized Burn Ratio (NBR) grid is derived through analysis of pre- and post-fire satellite images and the associated reflectance values of individual grid cells (Key and Benson, 2003). An NBR grid could

have provided an increased level of detail regarding burn severity, which may be an essential component of accurate post-fire hydrologic modeling.

While the DHSVM validation efforts were inconclusive, the results of the model version comparison were more promising. In the post-fire setting the DHSVM fire model outperformed DHSVM version 2.0.1 for each of the three simulated water years. These results suggest that the DHSVM fire model may be a more appropriate tool for hydrologic modeling in fire-affected watersheds.

Visual analysis of the simulated hydrographs (Figures 16 and 17) suggests that the fire model outperformed version 2.0.1 for each of the three snowmelt seasons, and particularly in 2005 and 2006. The calculated model statistics generally support this assessment (Table 6). The DHSVM fire model *MdAE* values were closer to zero, indicating a slightly better fit, for each of the three simulated snowmelt seasons. In 2005, visual examination of the hydrographs suggests that DHSVM version 2.0.1 did not fit the measured data in any way. And although both model versions produced unsatisfactory simulations in 2005, in comparison to DHSVM version 2.0.1, the DHSVM fire model provided a significantly improved simulation. This assessment is somewhat reflected in the calculated statistics. The *MdAE*, *EF**, and *E* statistics all indicate improved performance by the fire model; however, the *CD** value inaccurately suggests that DHSVM version 2.0.1 outperformed the fire model in 2005. In 2006, the only year available with significant variation in flow for the model to capture, the values for the three mean-objective functions (*RMSE*, *CD*, and *EF*) demonstrate a marked improvement in simulation accuracy produced by the DHSVM fire model when compared to DHSVM version 2.0.1 (Table 6).

In 2004, the statistics provide a mixed picture of model performance. The *MdAE*, *CD**, and *EF** values all indicate slightly better fit by the fire model version; however, the *E* values suggest the opposite (Table 6). This may be explained somewhat by examination of the hydrographs (Figures 16 and 17). In 2004, the DHSVM fire model simulated flow indicated a delayed onset of snowmelt runoff compared to what was measured and also to what was simulated by DHSVM version 2.0.1 However, once the fire model version began to simulate snowmelt runoff, this model version more closely matched the measured streamflow patterns for the remainder of 2004. This inconsistency of model performance is reflected in the calculated statistics.

There are a couple of potential explanations for the improved simulations provided by the DHSVM fire model version. The most significant difference between the version 2.0.1 and the fire model code, involves the static or dynamic nature of the soil and vegetation inputs. In DHSVM version 2.0.1, the vegetation and soil inputs are static. The model is not designed to allow for landscape disturbances in the middle of a simulation, and this version does not allow for any change in the vegetation over the course of a model run. As a result, the user must force the model to account for fire disturbances through manual alteration of the spatial inputs and the physical values characterizing them. In comparison, the DHSVM fire model incorporates code that enables the model to read in fire as a disturbance and to subsequently account for the effect of this disturbance on the soil and vegetation. Therefore, the soil and vegetation inputs used in this version of DHSVM are dynamic. This is advantageous in that the model manipulates the spatial data internally, based on logic imbedded in the code.

Another advantage is that because the soil and vegetation inputs are dynamic, the fire model allows for the recovery of these resources for every year following a fire.
In addition, the internal logic built into the DHSVM fire model code may provide a more stratified, and potentially more accurate, physical characterization of the vegetative cover present after a fire of mixed severity. This may lead to improved hydrologic simulations using the DHSVM fire model in fire-affected watersheds.

Another key issue with the post-fire application is that the sample size of snowmelt seasons is particularly small. 3-yrs, or three seasons of snowmelt data, in all likelihood, will not capture the dynamic range of annual variations in streamflow. Therefore, a sample of this size will not truly test the ability of a model to accurately simulate flows for a particular watershed. The results of this research indicate a slight decline in model performance in the post-fire setting. In addition, the results suggest a marked improvement in the post-fire simulations produced by the DHSVM fire model, compared to the simulations produced by DHSVM version 2.0.1. However, due to the limited sample size, these same trends can not be inferred for the population. Post-fire applications of both model versions using longer periods of streamflow data, under altered meteorological conditions, or for a different watershed may produce contradictory results.

7. CONCLUSION

Overall, the calibration of DHSVM version 2.0.1 to the Eightmile Creek watershed was successful. *MdAE* statistics calculated for each of six simulated water years were within the target threshold of < 50%. In comparison, model validation efforts were not as conclusive. A slight decline in model performance was observed for simulations following the fire; however, post-fire weather conditions and streamflow data availability were not as conducive to rigorous comparison of modeled to measured flow.

Based on the marked improvement in the accuracy of simulated streamflow following rigorous model calibration, this research suggests that calibration to some extent is a essential first step to the application of DHSVM to a particular watershed. Because the model is exceptionally sensitive to certain parameters (e.g. saturated hydraulic conductivity and reference height) it is imperative that these parameters be accurately adjusted to the research area in order to obtain accurate hydrologic simulations. A well-calibrated model should have a degree of regional translatability, and the calibrated parameters should theoretically be applicable to other watersheds of similar area, climatic patterns, vegetative structure, and dominant soil types. Because the hydrologic data needed to calibrate a model to a particular watershed are often not available, this research suggests that in order to produce reliable simulations, at very least, DHSVM should first be calibrated to a comparable watershed with available streamflow data prior to simulating streamflow for the watershed of interest.

Another key issue highlighted by this research is the use of statistics to quantify goodness-of-fit of simulated to measured streamflow data. The statistical assessment of the model performance for the calibration, validation, and version comparison efforts was

comprehensive. It was necessary to calculate a number of different statistics in order to accurately quantify the performance of the DHSVM simulations because of the variability in the shape of the hydrograph between individual water years, as well as between pre- and post-fire conditions.

The 1959 water year simulation data illustrate this point. Initial visual assessment of this graph indicates very poor or no model fit to measured streamflow. The median-based statistics support this assertion. However, closer examination reveals that the overall visual impression of the model simulation for this year is greatly affected by a few abnormally high outliers. Because the median value of a distribution is less sensitive to outliers than the mean value, the median-based goodness-of-fit statistics calculated for the 1959 water year give a more accurate representation of the true nature of the fit of the simulated data to the measured data. This illustrates the necessity of calculating multiple different statistics when assessing goodness-of-fit of hydrologic simulations. Accurate conclusions can not be drawn from one statistic alone, but instead, the convergence of multiple statistical measures is needed to draw realistic conclusions from the comparison of simulated to measured hydrologic data.

Despite the specific limitations of the post-fire simulations, the validation and version comparison exercises provided some insight into the use of DHSVM in fire-affected landscapes, as well as an illustration of the potential for improved simulations produced by the DHSVM fire model. Future research involving post-fire applications of both DHSVM version 2.0.1 and the DHSVM fire model to forested, mountainous catchments in western Montana is warranted. Specifically, post-fire research utilizing robust and distributed meteorological data, longer-term and continuous post-fire streamflow data,

and a high-resolution burn severity grid would help to address some of the key questions raised by this research with respect to the use of either version of DHSVM to model hydrologic response in a forested watershed following fire.

8. WORKS CITED

Agee, J.K. 1993. *Fire Ecology of Pacific Northwest Forests*. Island Press: Washington D.C.; 505.

Alexander, R.R., C.A. Troendle, M.R. Kaufmann, W.D. Shepperd, G.L. Crouch, and R.K. Watkins. 1985. *The Fraser Experimental Forest, Colorado: research program and published research 1937 – 1985, USDA Forest Service General Technical Report RM-118*. Rocky Mtn. For. and Range Exp. Stn.: Fort Collins, CO; 44.

Alila, Y., and J. Beckers. 2001. Using numerical modelling to address hydrologic forest management issues in British Columbia. *Hydrol. Process.* ***15***: 3371 – 3387.

Anderson, E.A. 1976. A point energy and mass balance model of snow cover. *NWS Technical Report 19*. National Oceanic and Atmospheric Administration: Washington D.C.; 150.

Berris, S.N., and R.D. Harr. 1987. Comparative snow accumulation and melt during rainfall in forested and clear-cut plots in the western Cascades of Oregon. *Wat. Resour. Res.* ***23***: 135 – 142.

Beven, K.J. 1984. Infiltration into a class of vertically non-uniform soils. *Hydrol. Sci. J.* ***29***(4): 425 – 434.

Bowling, L.C., and D.P. Lettenmaier. 1997. Evaluation of the effects of forest roads on streamflow in Hard and Ware Creeks, Washington. *Water Resources Series Technical Report 155*. U. Washington: Seattle; 202.

Brakensiek, D.L., W.J. Rawls, and G.R. Stephenson. 1986. Determining the saturated hydraulic conductivity of a soil containing rock fragments. *Soil Sci. Soc. Am. J.* ***50***(3): 834 – 835.

Bristow, K.L., and G.S. Campbell. 1984. On the relationship between incoming solar radiation and daily maximum and minimum temperature. *Agric. For. Meteorol.* ***31***: 159 – 166.

Brooks, R.J., and A.T. Corey. 1964. Hydraulic properties of porous media. *Hydrol. Pap.* ***3***. Colorado State Univ.: Fort Collins; 27.

Brooks, K.N., P.F. Ffolliott, H.M. Gregersen, and L.F. DeBano. 1997. *Hydrology and the Management of Watersheds*, 2nd edn. Iowa State U. Press: Ames; 502.

Brunt, D. 1932. Notes on radiation in the atmosphere. *Quarterly J. Royal Meteorological Soc.* ***58***: 389 – 420.

Brutsaert, W. 1975. On a derivable formula for long-wave radiation from clear skies. *Wat. Resour. Res.* ***11***(5): 742 – 744.

Campbell, G.S., and J.M. Norman. 1989. The description and measurement of plant canopy structure. In *Plant canopies: their growth, form, and function*, P.G. Jarvis (ed.). Cambridge University Press: Cambridge, UK; 1 – 19.

Christner, J., and R.D. Harr. 1982. Peak stream flows from the transient snow zone, Western Cascades, Oregon. *Proc. West. Snow Conf*. ***50***: 127 – 138.

Coffey, M.E., S.R. Workman, J.L. Taraba, and A.W. Fogle. 2004. Statistical procedures for evaluating daily and monthly hydrologic model predictions. *Trans. Am. Soc. Ag. Eng.* ***47***(1): 59-68.

Collares-Pereira, M., and A. Rabl. 1979. The average distribution of solar radiation – correlations between diffuse and hemispherical and between daily and hourly insolation values. *Solar Energy* ***22***(2): 155-164.

Cosgrove, B., and M. Rodell. Updated 17 August 1999. *LDAS Vegetation Parameters Mapped to UMD Classification Scheme*. NASA/GSFC. <http://ldas.gsfc.nasa.gov/LDAS8th/MAPPED.VEG/LDASmapveg.shtml> Accessed February 2006.

Costa-Cabral, M.C., and S.J. Burges. 1994. Digital elevation model networks (DEMON): A model of flow over hillslopes for computation of contributing and dispersal areas. *Wat. Resour. Res.* ***30***(6): 1681 – 1692.

DHSVM Administrator. Updated 28 February 2006A. *Distributed Hydrology Soil Vegetation Model*. Land Surface Hydrology Research Group, U. Washington: Seattle. <http://www.hydro.washington.edu/Lettenmaier/Models/DHSVM/index.shtml> Accessed 31 October 2006.

DHSVM Administrator. Updated 3 March 2006B. *Distributed Hydrology Soil Vegetation Model, Frequently Asked Questions*. Land Surface Hydrology Research Group, U. Washington: Seattle. <http://www.hydro.washington.edu/Lettenmaier/Models/DHSVM/faqs.shtml> Accessed 30 October 2006.

Daly, C., R.P. Neilson, and D.L. Phillips. 1994. A statistical-topographic model for mapping climatological precipitation over mountainous terrain. *J. Applied Meteor.* ***33***: 140 – 158.

DeBano, L.F. 2000. Water repellency in soils: a historical overview. *J. Hydrol*. ***232***: 4 – 32.

Desborough, C.E., and A.J. Pitman. 1998. The BASE land surface model. *Glob. Planet. Change* ***19***: 3 – 18.

Dickinson, R.E., A. Henderson-Sellers, and P.J. Kennedy. 1993. *Biosphere-Atmosphere Transfer Scheme (BATS) Version 1e as Coupled to the NCAR Community Climate Model: NCAR Technical Note, NCAR/TN-387+STR*. National Center for Atmospheric Research: Boulder, CO; 72.

Dickinson, R.E., A. Henderson-Sellers, C. Rosenzweig, and P.J. Sellers. 1991. Evapotranspiration models with canopy resistance for use in climate models, a review. *Agric. For. Meteorol.* ***54***: 373 – 388.

Doten, C.O. *et al*. 18 August 2004. *Hydrologic Modeling and DHSVM* [presentation]. Land Surface Hydrology Research Group, U. Washington: Seattle. <http://www.hydro.washington.edu/Lettenmaier/Presentations/2004/wood_dhsvm overview_FSmtg_aug04.ppt#261,1,Hydrologic Modeling and DHSVM> Accessed 7 November 2006.

Doten, C.O. and D.P. Lettenmaier. 2004. Prediction of sediment erosion and transport with the Distributed Hydrology-Soil-Vegetation Model. *Water Resources Series Technical Report Number 178*. U. Washington: Seattle; 63.

Doten, C.O., L.C. Bowling, J.S. Lanini, E.P. Maurer, and D.P. Lettenmaier. 2006. A spatially distributed model for the dynamic prediction of sediment erosion and transport in mountainous forested watersheds. *Wat. Resour. Res*. ***42***(4).

Eagleson, P.S. 1970. *Dynamic Hydrology*. McGraw-Hill: New York; 462.

Fisher, F.B., J.C. Winne, M.M. Thornton, T.P. Tady, Z. Ma, M.M. Hart, and R.L. Redmond. 1998. *Montana Land Cover Atlas: The Montana gap analysis project*. Wildlife Spatial Analysis Lab, Montana Cooperative Wildlife Research Unit, U. Montana: Missoula.

Fleming, M., and V. Neary. 2004. Continuous hydrologic modeling study with the hydrologic modeling system. *ASCE J. Hydrol. Eng.* ***9***(3): 175 – 183.

Fluker, B.J. 1958. Soil temperatures. *Soil Science* ***86***: 35 – 46.

Grayson, R., and G. Blöschl. 2000. *Spatial Patterns in Catchment Hydrology: Observations and Modelling*. Cambridge University Press: Cambridge, UK.

Harr, R.D. 1981. Some characteristics and consequences of snowmelt during rainfall in western Oregon. *J. Hydrol*. ***53***: 277 – 304.

Harr, R.D. 1986. Effects of clear-cut logging on rain-on-snow runoff in western Oregon: a new look at old studies. *Wat. Resour. Res.* ***22***: 1095 – 1100.

Harr, R.D., W.C., Harper, and J.T. Krygier. 1975. Changes in storm hydropgraphs after road building and clear cutting in the Oregon Coast Range. *Wat. Resour. Res.* ***11***: 436 – 444.

Hellweger, F. Updated 10 January 1997. AGREE – DEM surface reconditioning system. University of Texas <http://www.ce.utexax.edu/prof/maidment/GISHYDRO/ferdi/research/agree/agree.html#Part1> Accessed March 2007.

Hillel, D. 1980. *Fundamentals of Soil Physics*. Academic Press: New York; 413.

Jones, J.A., and G.E. Grant. 1996. Peak flow responses to clearcutting and roads in small and large basins, western Cascades, Oregon. *Wat. Resour. Res.* ***32***: 959 – 974.

Jury, W.A., and R. Horton. 2004. *Soil Physics*. Wiley: Hoboken, NJ; 384.

Kaufmann, M.R. 1982. Leaf conductance as a function of photosynthetic photon flux density and absolute humidity difference from leaf to air. *Plant Physiol.* ***69***: 1018 – 1022.

Kenward, T., and D.P. Lettenmaier. 1997. Assessment of required accuracy of digital elevation data for hydrological modeling. *Water Resources Series Technical Report Number 153*. U. Washington: Seattle; 131.

Key, C., and N.C. Benson. Updated 25 April 2003. The normalized burn ration (NBR): A Landsat TM radiometric measure of burn severity. USGS Northern Rocky Mtn. Science Center. <http://www.nrmsc.usgs.gov/research/ndbr.htm> Accessed December 2006.

Krause, P., D.P. Boyle, and F. Bäse. 2005. Comparison of different efficiency criteria for hydrological model assessment. *Advances in Geosciences* ***5***: 89 – 97.

Lanini, J.S. 2005. Effects of climate and fire regime on post-fire sediment delivery in Pacific Northwest forests. *M.S. Thesis*. U. Washington: Seattle; 55.

Laramie, R.L., and J.C. Schaake, Jr. 1972. Simulation of the continuous snowmelt process. In *Ralph M. Parsons Laboratory Report Number 143*. Massachusetts Institute of Technology: Cambridge.

Legates, D.R., and G.J. McCabe, Jr. 1999. Evaluating the use of "goodness-of fit" measures in hydrologic and hydroclimatic model validation. *Wat. Resour. Res.* ***35***(1): 233 – 241.

Linacre, E. 1992. *Climate Data and Resources: A Reference and Guide*. Routledge: New York; 384.

Loague, K.M., R.E. Green, and L.A. Mulkey. 1988. Evaluation of mathematical models of solute migration and transformation: An overview and an example. In *Proc. of the International Conf. and Workshop on the Validation of Flow and Transport Models for the Unsaturated Zone*. U. New Mexico: Albuquerque; 231 – 247.

Lolo Burned Area Emergency Recovery Team. 2003. Burned Area Emergency Response (BAER) Team Executive Summary: Cooney Ridge Fire, Lolo National Forest, Missoula, MT. USDA For. Serv.: Missoula; 8.

MacDonald, L.H. 2000. Evaluation and managing cumulative effects: process and constraints. *Environmental Management **26***: 299 – 315.

Maidment, D.R. 1993. *Handbook of Hydrology*. McGraw-Hill: New York; 1424.

Marsh, P. 1999. Snowcover formation and melt: recent advances and future prospects. *Hydrol. Process. **13***: 2117 – 2134.

McClelland, D.E., R.B. Foltz, C.M. Falter, W.D. Wilson, T. Cundy, R.L. Schuster, J. Saurbier, C. Rabe, and R. Heinemann. 1999. Relative effects on a low-volume road system of landslides resulting from episodic storms in Northern Idaho. In *Transportation Research Record, v2*(n1652). Presented at the 7th Intl. Conference on Low-Volume Roads, 23 – 26 May 1999: 235 – 243.

Mitchell, K.E., D. Lohmann, P.R. Houser, E.F. Wood, J.C. Schaake, A. Robock, B.A. Cosgrove, J. Sheffield, Q. Duan, L. Luo, R.W. Higgins, R.T. Pinker, J.D. Tarplay, D.P. Lettenmaier, C.H. Marshall, J.K. Entin, M. Pan, W. Shi, V. Koren, J. Meng, B.H. Ramsay, and A.A. Bailey. 2004. The multi-institution North American Land Data Assimilation System (NLDAS): Utilizing multiple GCIP products and partners in a continental distributed hydrological modeling system. *J. Geophys. Res. **109***.

Myneni, R.B., R.R. Nemani, and S.W. Running. 1997. Estimation of global leaf area index and absorbed par using radiative transfer models. *IEEE Trans. Geoscience Rem. Sens. **35***(6): 1380 – 1391.

Nash, J.E., and J.V. Sutcliffe. 1970. River flow forecasting through conceptual models: Part I – A discussion of principles. *J. Hydrol. **10***: 282 – 290.

National Oceanic and Atmospheric Administration. Updated November 2006. National Climatic Data Center Online.<http://cdo.ncdc.noaa.gov/CDO/cdo> Accessed November 2006.

Natural Resources Conservation Service. Updated February 10 2006A. Snow & Precipitation Data, Black Pine SNOTEL station. USDA NRCS. <http://www.mt.nrcs.usda.gov/snow/data/> Accessed 2006.

Natural Resources Conservation Service. Updated June 2006B. Basin-wide Snowpack Summary. USDA NRCS National Water and Climate Center. <http://www.wcc.nrcs.usda.gov/cgbin/snow_rpt.pl?state=montana> Accessed December 2006.

Nicks, A.D., and G.A. Gander. 1995. Weather Generator. In *USDA-Water Erosion Prediction Project Hillslope Profile and Watershed Model Documentation, NSERL Report Number 10*, Flanagan and Nearing (eds.). USDA National Soil Erosion Research Laboratory: Lafayette, IN.

Oke, T.R. 1988. *Boundary Layer Climates*, 2nd edn. Methuen & Co, Ltd.: New York; 450.

Putz, G., J.M. Burke, D.W. Smith, D.S. Chanasyk, E.E. Prepas, and E. Mapfumo. 2003. Modelling the effects of boreal forest landscape management upon streamflow and water quality: Basic concepts and considerations. *J. Environ. Eng. Sci.* ***2(***S1): S87 – S101.

Raines, G.L., and B.R. Johnson. 1995. Digital representation of the Montana state geologic map in ARC/INFO export format: U.S. Geological Survey Open-File Report 95-0691. USGS: Helena.

Ramakrishna, N. 2003. Production system planning for natural resource conservation in a micro-watershed. *Electronic Green Journal* **18**. <http://egj.lib.uidaho.edu/egj18/nallathiga1.html> Accessed 1/03/2007.

Rawls, W.J. 1983. Estimating soil bulk density from particle size analysis and organic matter content. *Soil Science* ***135***(2): 123 – 125.

Rawls, W.J. and D.L. Brakensiek. 1985. Prediction of soil water properties for hydrologic modeling. In *Watershed Management in the Eighties*, E. Jones and T.J. Ward (eds.). ASCE: Denver, CO; 293 – 299.

Reid, L.M. 1993. Research and cumulative watershed effects. *USDA For. Serv. Gen. Tech. Rep. PSW-GTR-141*. USDA Forest Service: Albany, CA; 118.

Roberts, M. 2006. Eightmile Creek Aquarod data. MT Department of Natural Resources and Conservation, Water Management Bureau. Personal communication.

Satterlund, D.R., and H.F. Haupt. 1967. Snow catch by conifer crowns. *Wat. Resour. Res*. ***3***: 1035-1039.

Schmidt, R.A., and D.R. Gluns. 1991. Snowfall interception on branches of three conifer species. *Canadian J. For. Res.* ***21***: 1262-1269.

Shuttleworth, W.J., and J.S. Wallace. 1985. Evaporation from sparse crops – an energy combination theory. *Quarterly J. Royal Meteorological Soc.* ***111***: 839-855.

Singh, V.P., and D. Frevert. 2002. *Mathematical Models of Large Watershed Hydrology*. Water Resources Publications: Chelsea, MI; 891.

Soil Survey Staff. Updated 1994. State Soil Geographic (STATSGO) database for Montana <http://nris.mt.gov/nsdi/nris/shape/ss19.zip> USDA NRCS: Helena. Accessed February 2006

Soil Survey Staff. 1999. Soil Taxonomy: A basic system of soil classification for making and interpreting soil surveys. *USDA NRCS Agriculture Handbook Number 436*, 2nd edn. USDA NRCS.

Soil Survey Staff. Updated 2006. Soil Survey Geographic (SSURGO) Database for Missoula County, MT. USDA NRCS: Helena. <http://soildatamart.nrcs.usda.gov> Accessed February 2006.

Spokas, K., and F. Forcella. 2006. Estimating hourly incoming solar radiation from limited meteorological data. *Weed Science* ***54***: 182 – 189.

Storck, P. 2000. Trees, snow, and flooding: An investigation of forest canopy effects on snow accumulation and melt at the plot and watershed scales in the Pacific Northwest. *PhD dissertation*. U. Washington: Seattle; 169.

Storck, P., and D.P. Lettenmaier. 1999. Predicting the effect of a forest canopy on ground snow accumulation and ablation in maritime climates. In *Proc. 67th Western Snow Conf.*, C. Troendle (ed.). Colorado State U.: Fort Collins: 1 – 12.

Storck, P., and D.P. Lettenmaier. 2000. Trees, snow and flooding: an investigation of forest canopy effects on snow accumulation and melt at the plot and watershed scales in the Pacific Northwest. *Water Resources Series Technical Report Number 161*. U. Washington: Seattle.

Storck, P., L. Bowling, P. Weatherbee, and D.P. Lettenmaier. 1998. Application of a GIS based distributed hydrology model for prediction of forest harvest effects on peak stream flow in the Pacific Northwest. *Hydrol. Process.* ***12***: 889 – 904.

Strahler, A.N. 1952. Hypsometric (area-altitude) analysis of erosional topography. *Geol. Soc. Am. Bull.* ***63***: 1117 – 1142.

Tangedahl, E. 2006. Utilization of the Distributed Hydrology-Soil-Vegetation Model (DHSVM) to quantify streamflow changes and slope failure probability following the snow-talon fire near Lincoln Montana, USA. *M.S. Thesis*. U. Montana: Missoula; 53.

Thornton, P.E., H. Hasenauer, and M.A. White. 2000. Simultaneous estimation of daily solar radiation and humidity from observed temperature and precipitation: an application over complex terrain in Austria. *Ag. For. Meteor.* ***104***: 255 – 271.

Thornton, P.E., and S.W. Running. 1999. An improved algorithm for estimating incident daily solar radiation from measurements of temperature, humidity, and precipitation. *Ag. and For. Meteor.* ***93***: 211 – 228.

Thornton, P.E., S.W. Running, and M.A. White. 1997. Generating surfaces of daily meteorological variables over large regions of complex terrain. *J. Hydrology* ***190***: 214 – 251.

Thyer, M., J. Beckers, D. Spittlehouse, Y. Alila, and R. Winkler. 2004. Diagnosing a distributed hydrologic model for two high-elevation forested catchments based on detailed stand- and basin-scale data. *Wat. Resour. Res.* ***40***: 1 – 20.

Troendle, C.A., and R.M. King. 1985. Effect of timber harvest on the Fool Creek Watershed, 30 years later. *Wat. Resour. Res.* ***21***(12): 1915 – 1922.

United States Geological Survey. Updated 2002. National Elevation Dataset. Natural Resource Information System, Montana State Library: Helena. <http://nris.mt.gov/nsdi/ned/html> Accessed 2005.

United States Geological Survey. Updated 2005. USGS 12351400 Eightmile Creek near Florence MT. Montana Water Science Center, National Water Information System. <http://waterdata.usgs.gov/nwis/inventory/?site_no=12351400> Accessed June 2005.

United States Geological Survey and United States Environmental Protection Agency. Updated 2000. National Hydrography Dataset. Natural Resource Information System, Montana State Library: Helena.<http://nris.state.mt.us/nsdi/nhd/nhd_drain.zip> Accessed 2006.

VanShaar, J.R., I. Haddeland, and D.P. Lettenmaier. 2002. Effects of land-cover changes on the hydrological response of interior Columbia River basin forested catchments. *Hydrol. Process.* ***16***: 2499 – 2520.

Ward, A.D., and W.J. Elliot. 1995. *Environmental Hydrology*. Lewis Publishers: New York; 496.

Waring, R.H, and W.H. Schleshinger, 1985. *Forest Ecosystems: Concepts and Management*. Academic Press: Orlando, FL; 340.

Western Regional Climate Center. Updated 2002. Historical Climate Information. <http://www.wrcc.dri.edu/htmlfiles/westwind.final.html> Accessed January 2006.

Whitaker, A., Y. Alila, J. Beckers, and D. Toews. 2003. Application of the distributed hydrology soil vegetation model to Redfish Creek, British Columbia: model evaluation using internal catchment data. *Hydrol. Process.* ***17***(1): 199 – 224.

Wigmosta, M.S. and W.A. Perkins. 2001. Simulating the effects of forest roads on watershed hydrology. In *Land Use and Watersheds: Human Influence on Hydrology and Geomorphology in Urban and Forest Areas*, M.S. Wigmosta and S.J. Burges (eds.). *AGU Water Science and Application* ***2***: 127 – 143.

Wigmosta, M.S., B. Nijssen, P. Storck, and D.P. Lettenmaier. 2002. The Distributed Hydrology Soil Vegetation Model. In *Mathematical Models of Small Watershed Hydrology and Applications*, V.P. Singh and D.K. Frevert (eds.) Water Resource Publications: Littleton, CO; 7 – 42.

Wigmosta, M.S., L.W. Vail, and D.P. Lettenmaier. 1994. Distributed hydrology vegetation model for complex terrain. *Wat. Resour. Res*. ***30***(6): 1665 – 1679.

Wilson, M.F., and A. Henderson-Sellers. 1985. A global archive of land cover and soils data for use in general circulation climate models. *J. Climatology* ***5***: 119 – 143.

Wohl, E. 2000. *Mountain Rivers*. American Geophysical Union: Washington, D.C.; 320.

Woods, J. 2005. Plum Creek Roads digital data. Plum Creek Timber Company: Missoula.

Yeh, G., G. Huang, H. Cheng, F. Zhang, H. Lin, E. Edris, and D. Richards. 2006. A first principle, physics-based watershed model: WASH123D. In *Watershed Models,* V.P. Singh and D.K. Frevert (eds.). Taylor and Francis: Boca Raton, FL; 211 – 244.

Zacharias, S., C.D. Heatwole, and C.W. Coakley. 1996. Robust quantitative techniques for validating pesticide transport models. *Trans. ASAE* ***39***(1): 47 – 54.

9. APPENDIX

Table A1 – *Constants*.

PARAMETER	DESCRIPTION	VALUE	UNIT	SOURCE
Ground Roughness	aerodynamic roughness of soil surface	0.025	m	Maidment, 1993
Snow Roughness	aerodynamic roughness of snow surface	0.01	m	Desborough and Pitman, 1998
Rain Threshold	temperature above which all precipitation falls as rain	-0.5	°C	none needed
Snow Threshold	temperature below which all precipitation falls as rain	-0.5	°C	none needed
Snow Water Capacity	snow liquid WHC	0.01	unitless	Brooks et al., 1997
Reference Height	reference height for wind calculations	40	m	none needed
Rain LAI multiplier	LAI multiplier for rain interception	0.0001	unitless	Storck, 2000
Snow LAI multiplier	LAI multiplier for snow interception	0.0005	unitless	Storck, 2000
Min Intercepted Snow	intercepted snow that can only be melted	0.005	m	Storck, 2000
Temperature Lapse Rate	elevation-based temperature lapse rate	-0.0055	°C/m	Kenward and Lettenmaier, 1997
Precipitation Lapse Rate	elevation-based precipitation lapse rate	0.0002341	m/m	Natural Resources Conservation Service, 2006A

Table A2 – *Soil input parameters*.

PARAMETER	DESCRIPTION	UNIT	SOIL TYPE 1	SOIL TYPE 2	SOIL TYPE 3
Texture[10, 11]	dominant texture of soil profile	unitless	Gravelly Loam	Gravelly Silt Loam	Gravelly Sandy Loam
Lateral Conductivity[2, 6]	lateral saturated hydraulic conductivity	m/s	3.65E-05	1.88E-05	6.03E-05
Exponential decrease[1, 7]	exponent for change of lateral conductivity with depth	unitless	1.4	1.4	1.4
Maximum infiltration[3]	maximum infiltration rate	m/s	3.65E-05	1.88E-05	6.03E-05
Surface albedo[12]	albedo of bare soil surface	m/s	0.15	0.15	0.15
Number of soil layers[10, 11]	number of layers described in soil profile	unitless	4	4	4
Porosity[6, 9]	porosity of each soil layer	unitless	0.450 - 0.461	0.45 - 0.498	0.45 - 0.451
Pore size distribution[6, 9]	% of bulk volume of various sizes of soil pores for each soil layer	unitless	0.252 - 0.378	0.234 - 0.378	0.378
Bubbling pressure[6, 9]	air entry value for each soil layer	m	0.112 - 0.147	0.147 - 0.208	0.147
Field capacity[6, 9]	water retained at -1500 kPa for each soil layer	unitless	0.207 - 0.270	0.207 - 0.330	0.307
Wilting point[6, 9]	water retained at -33 kPa for each soil layer	unitless	0.095 - 0.117	0.095 - 0.133	0.095
Bulk density[6,8]	mass dry soil per unit bulk volume for each soil layer	kg/m^3	1245.5 - 1550.0	1099 - 1550	1550
Vertical conductivity	vertical saturated hydraulic conductivity for each soil layer	m/s	6.02E-05 - 3.65E-05	6.02E-05 - 1.88E-05	6.02E-05
Thermal conductivity[4, 5]	thermal conductivity of dry soil for each soil layer	W/m°C	1.511 - 1.622	1.402 - 1.622	1.622
Thermal capacity[5]	thermal capacity of dry soil for each soil layer	J/m^3°C	1.30E06 - 1.33E06	1.30E06 - 2.39E06	1.3E06

[1]Beven, 1984
[2]Brakensiek *et al.*, 1986
[3]Fleming and Neary, 2004
[4]Fluker, 1958
[5]Hillel, 1980
[6]Maidment, 1993
[7]Oke, 1988
[8]Rawls, 1983
[9]Rawls and Brakensiek, 1985
[10]Soil Survey Staff, 1994
[11]Soil Survey Staff, 2006
[12]Wilson and Henderson-Sellers, 1985

Table A3 – *Vegetation type descriptions*.

CLASS #	VEGETATION TYPE	% TOTAL AREA	GENERAL DESCRIPTION BY % COVER	DOMINANT TREE SPP.
1	Grasslands and meadows	9.5%	herbaceous cover > 10% shrub cover < 15% no forest cover	none
2	Open shrubland	<1%	herbaceous cover > 10% 15% < shrub cover > 50% no forest cover	none
3	Closed shrubland	10.1%	herbaceous cover > 10% shrub cover > 50% no forest cover	none
4	Wooded grassland	6.5%	herbaceous cover > 10% shrub cover < 15% 50% coniferous forest cover	*Pinus ponderosa, Pseudotsuga menziesii*
5	Mixed cover	<1%	herbaceous cover > 10% shrub cover < 15% 80% coniferous forest cover	*Pinus ponderosa, Pseudotsuga menziesii*
6	Deciduous broadleaf forest	<1%	herbaceous cover > 10% shrub cover < 15% 90% deciduous hardwood forest cover	*Populus tremuloides, Betula spp.*
7	Deciduous needleleaf forest	<1%	herbaceous cover > 10% shrub cover < 15% 80% deciduous softwood forest cover	*Larix occidentalis*
8	Evergreen needleleaf forest	71.5%	herbaceous cover > 10% shrub cover < 15% 50% forest cover	*Pinus ponderosa, Pseudotsuga menziesii*
9	Bare ground	<1%	0% herbaceous, shrub, and forest cover	none

Table A4 – *Vegetation input parameters*.

PARAMETER	DESCRIPTION	SOURCE
Fractional Coverage	the fraction of total area occupied by the overstory (unitless)	Thyer *et al.*, 2004
Trunk Space	distance from the ground to the start of the crown (m)	no sources available
Aerodynamic Attenuation	canopy attenuation coefficient for the wind profile (s/m)	Shuttleworth and Wallace, 1985
Radiation Attenuation	radiation attenuation by the overstory (unitless)	Wigmosta *et al.*, 1994
Maximum Snow Int Capacity	max snow interception capacity for the overstory (m SWE)	Storck, 2000; Satterlund and Haupt, 1967; Schmidt and Gluns, 1991; Whitaker *et al*., 2003
Max Release Drip Ratio	ratio of mass release to meltwater drip from intercepted snow (m SWE)	Storck, 2000
Snow Interception Efficiency	percentage of snowfall intercepted until the maximum snow interception capacity has been met (unitless)	Storck, 2000; Satterlund and Haupt, 1967; Schmidt and Gluns, 1991; Whitaker *et al.*, 2003
Height	height of each vegetation layer (m)	no sources available
Maximum Resistance	maximum stomatal resistance for each vegetation layer (s/m)	Alexander *et al.*, 1985; Kenward and Lettenmaier, 1997
Minimum Resistance	minimum stomatal resistance for each vegetation layer (s/m)	Alexander *et al.*, 1985
Moisture Threshold	value above which soil moisture does not restrict transpiration (unitless)	Maidment, 1993
Vapor Pressure Deficit	vapor pressure deficit threshold above which stomatal closure occurs (Pa)	Whitaker *et al*., 2003
Rpc	fraction of shortwave radiation that is photosynthetically active (W/m^2)	Dickinson *et al*., 1991
LAI Values	monthly LAI values for each vegetation type (unitless)	Alexander *et al.*, 1985; Cosgrove and Rodell, 1999; Mitchell *et al.*, 2004
Albedo Values	monthly albedo values for each vegetation type (unitless)	Cosgrove and Rodell, 1999; Myeni *et al.*, 1997; Kaufmann *et al.*, 1982; Eagleson, 1970

Table A5 – ***Summary of statistical measures of goodness-of-fit.***

STATISTIC	SYMBOL	RANGE	PERFECT FIT	TARGET FIT	SOURCE
Median Based Functions					
normalized median absolute error (%)[1]	*MdAE*	0 to 1	0	< 50%	Zacharias, *et al.*, 1996
robust coefficient of determination [2]	*CD**	-1 to 1	1	±0.5 from 1.0	Zacharias, *et al.*, 1996
robust modeling efficiency [3]	*EF**	-1 to 1	1	±0.5 from 1.0	Zacharias, *et al.*, 1996
Mean Based Functions					
Nash-Sutcliffe efficiency coefficient [4]	*E*	1 to -∞	1	> 0	Nash and Sutcliffe, 1970
normalized root mean square error (%) [5]	*RMSE*	0 to 1	0	< 50%	Loague *et al.*, 1988
coefficient of determination [6]	*CD*	-1 to 1	1	±0.5 from 1.0	Loague *et al.*, 1988
modeling efficiency value [7]	*EF*	-1 to 1	1	±0.5 from 1.0	Loague *et al.*, 1988

[1] $$MdAE = median\left\{\left|Y_i - X_i\right| : i = 1,2,\mathrm{K}\ ,n\right\} \times \left(\frac{100}{\overline{Y*}}\right)$$

[2] $$CD* = \frac{median\left\{\left|Y_i - \overline{Y*}\right| : i = 1,2,\mathrm{K}\ ,n\right\}}{median\left\{\left|X_i - \overline{Y*}\right| : i = 1,2,\mathrm{K}\ ,n\right\}}$$

[3] $$EF* = \frac{\left\{\left|Y_i - \overline{Y*}\right| : i = 1,2,\mathrm{K}\ ,n\right\} - median\left\{\left|Y_i - X_i\right| : i = 1,2,\mathrm{K}\ ,n\right\}}{median\left\{\left|Y_i - \overline{Y*}\right| : i = 1,2,...,n\right\}}$$

[4] $$E = 1 - \frac{\sum_{i=1}^{n}\left(Y_i - X_i\right)^2}{\sum_{i=1}^{n}\left(Y_i - \overline{Y}\right)^2}$$

[5] $$RMSE = \left[\left(\frac{1}{n}\right)\sum_{i=1}^{n}\left(Y_i - X_i\right)^2\right]^{0.5}\left(\frac{100}{\overline{Y}}\right)$$

[6] $$CD = \frac{\sum_{i=1}^{n}\left(Y_i - \overline{Y}\right)^2}{\sum_{i=1}^{n}\left(X_i - \overline{Y}\right)^2}$$

[7] $$EF = \frac{\sum_{i=1}^{n}\left(Y_i - \overline{Y}\right)^2 - \sum_{i=1}^{n}\left(Y_i - X_i\right)^2}{\sum_{i=1}^{n}\left(X_i - \overline{Y}\right)^2}$$

Where:
X refers to the simulated values and Y refers to the observed values.
$\overline{Y}$ is the mean of the observed values.
$\overline{Y*}$ is the median of the observed values.